



NTNU – Trondheim
Norwegian University of
Science and Technology

Biophysical Studies of Light Sensitive Chromophores in Rat Glioma and Chinese Hamster Ovary Cancer Cells

Monica Kløvstad Siksjø

MSc in Physics

Submission date: May 2015

Supervisor: Mikael Lindgren, IFY

Co-supervisor: Odrun Gederaas, IKM

Norwegian University of Science and Technology
Department of Physics

Preface

It was by chance that I stumbled upon the field of biophysics at the beginning of my two-year Master degree in the fall of 2013, and I have not regreted my academic change of direction once. I had never heard of photodynamic therapy before I started on my Master, but found the concept intriguing. The subject has proven to be very interesting, and I believe it to be a great option to radiotherapy and chemotherapy.

The work done would of course not have been possible without the invaluable guidance and training provided by my supervisors; Prof. Mikael Lindgren (Department of Physics, NTNU) and senior researcher Odrun A. Gederaas (Department of Cancer Research and Molecular Medicine, NTNU). I would also like to express special gratitude to Pål Ellingsen for help and guidance during my first year. To Thor Bernt Melø for training in the spectroscopy lab, to Kjartan Wøllo Egeberg and Bjørnar Spornsheim for help with the confocal microscope. Thanks to Siri Bachke for help and answering my questions. And of course, a special thanks to Cyrille Monnereau and his team at ÉNS Lyon; especially to Bastien Mettra for providing the chromophores and information about their syntesization process.

Abstract

The aim of this study was to investigate the biophysical properties of four light sensitive chromophores as a fluorescence dye for bioimaging applications, or photosensitizer in photodynamic therapy (PDT). Characterization of light induced cell death and DNA damage were performed using Chinese hamster ovary cancer cells (CHO-K1) after incubation of the anthracene compounds Ant-PIm and Ant-PHEA using the standard PDT technique; survival studies with MTT assay. Confocal microscopy was also performed including DRAQ5 and LysoTracker Red as reference molecules for detection of the localization of the chromophore in cell compartments and nucleus in rat glioma (F98) and Chinese hamster ovary (CHO-K1) cell lines. Spectroscopic measurements such as absorption, excited state absorption, and singlet oxygen luminescence were performed to investigate important and necessary properties of the dyes as potential photosensitizers.

One of the chromophores (Ant-PIm) showed promising results for PDT with accelerated cell death upon illumination, but in addition a high dark toxicity. None of the tested chromophores caused any large DNA damage in CHO-K1 cells alone, or in combination with light. Only the chromophore DBB₂-OAc showed the ability of having a long lived triplet state, and generation of singlet oxygen, making it a promising candidate for PDT. All four chromophores were proven to localize in the cell compartments in cytosol of both F98 and CHO-K1 cells, but not necessarily inside the cell nucleus.

This project was part of a collaborating study with ÉNS Lyon, France and NTNU, Norway.

Sammendrag

Målet med dette arbeidet var å undersøke de biologiske egenskapene til fire lyssensitive kromoforer som fluorescence fargestoff for biologisk avbildning, eller som fotosensitive forbindelse i fotodynamisk terapi (PDT). Lysindusert celledød og DNA-skade i kinesisk hamster eggstokkreftceller (CHO-K1) etter inkubering av antracenstoffene Ant-PIIm og Ant-PHEA ble karakterisert ved å bruke standard PDT-teknikk; overlevelsesforsøk med MTT-analyse. Konfokalmikroskopi ble utført med DRAQ5 og Lysotracker Red som referanse molekyler for deteksjon av lokaliseringen til kromoforene i celleorganeller og nukleus i rotteoglioma- (F98) og kinesisk hamster eggstokkreftceller (CHO-K1). Spektroskopiske målinger som absorbans, eksitert tilstand-absorbans og singlet oksygen luminescens ble utført for å undersøke kromoforenes viktige og nødvendige egenskaper som potensielle fotosensitive forbindelser.

Ett av kromoforene (Ant-PIIm) viste lovende resultater for PDT med økende celledød ved belysning, men i tillegg høy mørke toksisitet. Ingen av de testede kromoforene forårsaket en stor mengde DNA-skade i CHO-K1 celler alene eller i kombinasjon med lysbehandling. Bare kromoforet $\text{DBB}_2\text{-OAc}$ viste evnen til en triplett tilstand med relativ lang levetid, samt generering av singlet oksygen luminescens. Dette gjør den til en lovende kandidat for PDT. Alle fire kromoforene viste seg å lokalisere i celleorganeller i cytosol i både F98 og CHO-K1 celler, men ikke nødvendigvis i nukleusen.

Dette prosjektet var en del av et samarbeidsprosjekt mellom ÉNS Lyon, Frankrike og NTNU, Norge.

Abbreviations

ALS	Alkali-labile site
ATRP	Atom transfer radical polymerization
Bipy	2,2'-Bipyridine
EtBr	Ethidium bromide
CH₂Cl₂	Dichloromethane
CHO-K1	Chinese hamster ovary cell line
CuBr	Copper(I) bromide
CuI	Copper(I) iodide
dH₂O	Distilled water
DNA	Deoxyribonucleic acid
DMSO	Dimethyl sulfoxide
ESA	Excited state absorption
Et₃N	Triethylamine
F98	Rat glioma cell line
HAL	Hexyl 5-aminolevulinate acid
Hp	Hemaporphyrin
HpD	Hemaporphyrin derivative
KOH	Potassium hydroxide
LD₅₀	Mean lethal dose
MeOH	Methanol
mTHPC	<i>meso</i> -tetrahydroxyphenylchlorin
MTT mide	3-(4,5-dimethylthiazol-2-yl)-2,5-diphenyltetrazolium bro-
OD	Optical density
PBS	Phosphate-buffered saline

PdCl₂(PPh₃)₂	Bis(triphenylphosphine)palladium(II) dichloride
PDT	Photodynamic therapy
PMT	Photomultiplier tube
PS	Photosensitizer
Pyr	Pyridine
ROS	Reactive oxygen species
RT	Room temperature
SD	Standard Deviation
SSB	Single-strand break
THF	Tetrahydrofuran
TMSBr	Trimethylsilyl bromide

Contents

Preface	i
Abstract	iii
Abbreviations	vii
1 Introduction	1
1.1 Brief history	1
1.2 Photodynamic therapy	3
1.3 Purpose of study	3
1.4 Outline	4
2 Background and Theory	5
2.1 Cell lines used	5
2.1.1 F98 glioma	5
2.1.2 CHO-K1	6
2.2 The chromophores	7
2.3 Spectroscopy	9
2.3.1 Absorbance	11
2.3.2 Luminescence	12
2.4 Photodynamic therapy	15
2.5 Comet assay	19
2.6 Confocal laser scanning microscopy	19
2.6.1 Theory	19
2.6.2 Detecting of fluorochromes in cancer cells	21

3	Materials and Methods	23
3.1	Cell cultivation	23
3.2	The chromophores	24
3.3	MTT assay	24
3.4	PDT-experiment	24
3.4.1	Light source	24
3.4.2	Cell survival study - Experimental procedure of MTT assay	25
3.5	Comet assay	27
3.5.1	Experimental procedure	27
3.6	Confocal laser scanning microscopy	30
3.6.1	Experimental procedure	30
3.7	Spectroscopy	31
3.7.1	Absorbance	31
3.7.2	Excited state absorbance	31
3.7.3	Transient state lifetime	32
3.7.4	Singlet oxygen lifetime	32
4	Results	33
4.1	Cell death following PDT with continuous light delivery	33
4.2	Comet assay after Ant-PIm and Ant-PHEA induced PDT	36
4.3	Spectroscopy	38
4.3.1	Absorbance	38
4.3.2	Excited state absorbance	39
4.3.3	Transient state lifetime	42
4.3.4	Singlet oxygen lifetime	43
4.4	Localization of chromophores in F98 rat glioma cells	45
4.5	Localization of chromophores in CHO-K1 hamster ovary cells	50
4.6	Colocalization of chromophore and fluorescence stain	55
5	Discussion	59
5.1	CHO-K1 cell death following PDT with continuous light delivery	59
5.1.1	Ant-PIm	59
5.1.2	Ant-PHEA	60
5.1.3	CHO-K1 sensitivity to blue light	60

5.2	DNA damage following Ant-PIm and Ant-PHEA induced PDT	63
5.3	Spectroscopic measurements of DBB ₂ -OAc, Ant-PIm and Ant-PHEA	64
5.3.1	Absorbance	64
5.3.2	Excited state absorbance	64
5.3.3	Transient state lifetime	65
5.3.4	Singlet oxygen lifetime	65
5.4	Localization of chromophores in F98 and CHO-K1 cells	66
5.5	Chromophores as a potential photosensitizer	67
5.6	Future work	68
6	Conclusions	69
	Appendices	79
A	Recipes of media	80
A.1	Growth medium - F98 rat glioma cell line	80
A.2	Growth medium - CHO-K1 hamster ovary cell line	80
B	Reagents for Comet assay	81
B.1	1% normal melting agarose gel	81
B.2	1% low melting agarose gel	81
B.3	Lysis buffer with 10% DMSO and 1% Triton-X	81
B.4	Alkali electrophoresis buffer	82
B.5	Neutralizing buffer	82
C	Colocalization images	83
C.1	F98 rat glioma cells	84
C.2	CHO-K1 Chinese hamster ovary cells	87
D	Pilot studies of DBB₂-OAc	90
E	Chromophore synthesis process	91
F	Bürker chamber	94
G	PCI Biotech LumiSource	96

Introduction

1.1 Brief history

The combination of light and chromophores in order to cause photobiological effects in biological systems is not a new idea, in fact, photodynamic therapy (PDT) dates back over a hundred years. This toxic effect of PDT was first reported by von Tappenier's student Oscar Raab which found a lethal effect when exposing paramecium to a light absorbing dye and light. [1, 2] This effect was later used to treat cancer in a small clinical study by von Tappenier and Jesionek in 1905, by using eosin and white light on skin tumors. [3]

Light alone has also been used for treatment of diseases. Niels Rydberg Finsen was a pioner in the field of photodermatology. He treated over 800 patients with lupus vulgaris by the use of light in the end of the 18th century, and was awarded the Nobel Prize in medicine in 1903 for his work in phototherapy. [4]

The effect of hematoporphyrin (Hp) on humans was first studied by Meyer-Betz in 1913 when he injected himself with the porphyrin to prove photosensitivity. He and Fischer had previously, in 1912, already found photosensitivity in mice after incubation of Hp. [5] Policard discovered later in 1924 that Hp fluorescence has diagnostic capabilities. There was a lot of focus on porphyrins as photosensitizers (PS) after the discovery of selective uptake of Hp in animals tumors by Auler and Banzer in 1942. These results were confirmed by Figge,

Weiland and Manganiello in 1948. [2, 6, 7]

Further, the PDT era as we know it today started in 1960 when Lipson could report tumor fluorescence using hematoporphyrin derivative (HpD). [8] Diamond *et al.* conducted a study in 1972 to investigate if hematoporphyrin behaves as an selective PS and kills cancer cells when exposed to visible light. They found the combination of Hp and light to be lethal to glioma cells *in vitro*, and to tumor cells in rats 24 hours postincubation. Diamond stated that it was likely that cell death was caused by production of singlet oxygen. [9]

Dougherty found in a study in 1975 good long-term results from red light treatment of various types of cancers in mice and rats injected with Hp. [10] The same year Kelly and Snell tested HpD with light on bladder carcinoma from humans in mice, and results showed that tumors were severely damaged by the treatment. [6] One year later Kelly and Snell conducted the first clinical trial on humans using HpD. They found high intensity illumination of areas with HpD in bladder carcinoma led to tumor destruction. [11, 12] Dougherty and his team achieved complete response or partial response in 111 out of 113 malignant tumors in a clinical study in 1978 using HpD and red light on various cancer types. [13]

After this several clinical trials have been conducted for different types of malignant lesions using different types of photosensitizers. The results has been varying due to low specificity and potency of PS, along with the focus on advanced-stage diseases with no other treatment options. However, PDT has been given a lot of attention the last decades, and newer and better PS are being developed and investigated along with better localization methods potentially improving the efficacy of PDT. [12]

1.2 Photodynamic therapy

The outcome of PDT depends on the localization of the photosensitizer inside the cells. It may be in organelles such as mitochondria, lysosomes, or internal and plasma membranes, and the PDT-damages caused upon the cells depend on the subcellular compartments (Section 2.4). [14]

By *in vitro* studies DNA damage has been demonstrated as a consequence of PDT. It is important to note that this damage has not been directly linked to lethal effects. The DNA damage after PDT is generally believed to be related to base oxidative damage, strand breaks or cross-links. [15, 16]

After PDT the cells might undergo *apoptosis* or *necrosis*. Apoptosis is rapid programmed cell death following irradiation. The nucleus will show characteristic densely staining globules, and some of the DNA is broken down into internucleosomal units. Apoptosis is a way to eliminate cells with damaged DNA that were not repaired properly. [17] Necrosis is accidental, and often follows massive tissue injury (such as mechanical trauma or exposure to a toxic agent). The damage is too severe for the cell to maintain its level of normal activity, and falls apart. [18]

Different factors are important in determination of type of cell death after treatment: cell type, subcellular localization of the photosensitizer, and dose of light used during illumination. It is generally believed that apoptosis follows photodamage caused by PS localized in mitochondria, while necrosis follows photodamage caused by PS localized in plasma membranes. [14]

1.3 Purpose of study

The aim of the thesis work was to investigate the PDT efficiency of new chromophores synthesized by a group at ÉNS (Écoles Normales Supérieures) Lyon, France. The master thesis is a part of an ongoing study with collaboration between NTNU in Norway and ÉNS. Data about the chromophores were collected using survival assays on cell models, and spectroscopic and microscopic methods.

It was of great interest to localize the chromophores in different cell models (F98 rat glioma and CHO-K1 hamster ovary), and also their effectiveness

as a photosensitizer leading to cell death. By using confocal laser scanning microscopy on chromophore-incubated cells a detailed study for localizing the chromophores were performed. Cell survival experiments (MTT) were conducted 24 h post-PDT to investigate some of the most promising chromophores' abilities as a PS, while comet assay was performed to document DNA damage after PDT. The triplet state absorption was investigated using excited state absorption spectroscopy (ESA), and the singlet oxygen lifetime was recorded using singlet oxygen luminescence, since singlet oxygen ($^1\text{O}_2$) is generally believed to be the number one reason for cell death following PDT. The other possibility may be other reactive oxygen species (ROS).

The results achieved in the master thesis are important information about the new chromophores, and will be used for further development of the study which will continue afterwards.

1.4 Outline

In *Chapter 2* information about the relevant cancer cell lines and chromophores are given, along with basic theory of spectroscopy and the relevant techniques performed in the thesis work. The basic theory of photodynamic therapy, the comet assay, and confocal laser scanning microscopy are also elaborated in this chapter.

In *Chapter 3* the performed methods (PDT experiment with consecutive MTT assay, comet assay, confocal laser scanning microscopy, absorbance spectroscopy, excited state absorbance, and singlet oxygen luminescence) are described along with information about cell cultivation and storage of the chromophores.

In *Chapter 4* the results are presented.

In *Chapter 5* the results are discussed, and compared to recent research done in the field.

In *Chapter 6* the conclusions are given.

Background and Theory

2.1 Cell lines used

Two different cell lines were used in the thesis; F98 rat glioma, and CHO-K1 Chinese hamster ovary. Pilot studies had been conducted by co-supervisor Odrun Gederaas using F98 cell line (Appendix D), the same cell line was used for the first confocal laser scanning microscopy experiments.

Later it came of interested to perform experiments using CHO-K1 Chinese hamster ovary cell line, and that cell line was mostly used in the present work.

2.1.1 F98 glioma

Tumor models from rats have been widely used in experimental research for almost 40 years. Even though they do not simulate the human brain exactly, they have proven to be a resourceful model to get information about biochemical and biological properties of brain tumors in both *in vitro* and *in vivo*.

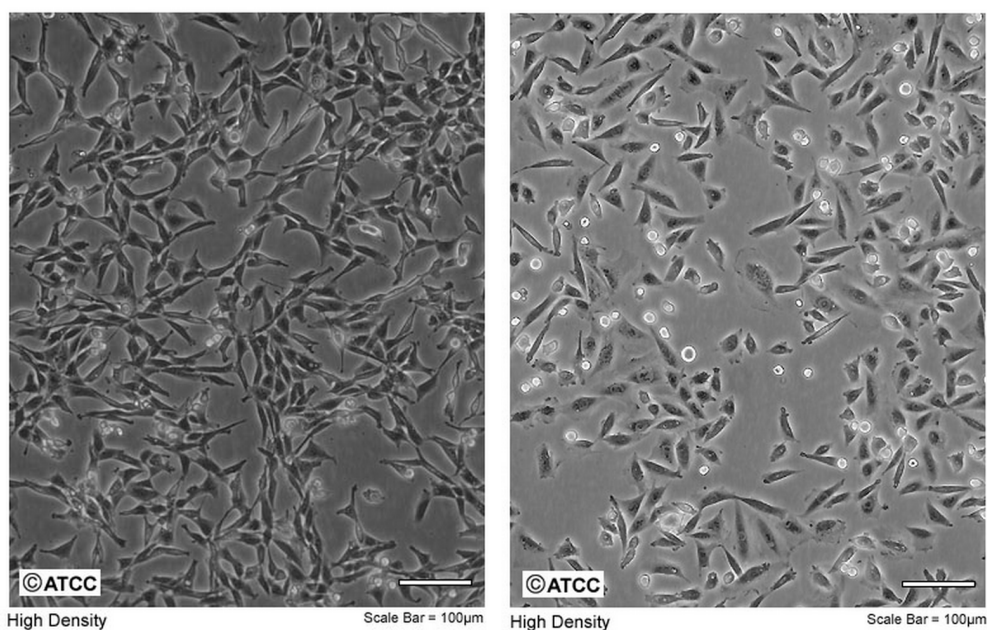
The F98 glioma model is a chemically induced rat tumor and has shown to resemble human glioblastoma to a great extent. Both have an infiltrative pattern of growth in the brain, both are very weakly immunogenic, and both are extremely lethal.

This model is very attractive for testing of new therapeutic modalities due to its invasive pattern of growth and uniform lethality from very few cells, in addition to the resemble to human tumors. [19] The F98 glioma cell line has a

doubling time of ~ 16 h. [20]

2.1.2 CHO-K1

CHO-K1 is a Chinese hamster ovary (CHO) cell line, and were first isolated in 1957 by T. T. Puck. [21] The Chinese hamster cell line is particularly sturdy and reliable, and the cells can be cultured continuously for several months with no reduction in growth rate, or change in cellular or colonial morphology. [22] The CHO-K1 ovary cell line has a doubling time of ~ 12 h. [23]



(a) F98 - rat glioma

(b) CHO-K1 - Chinese hamster ovary

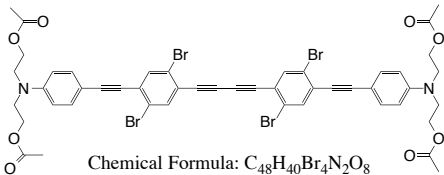
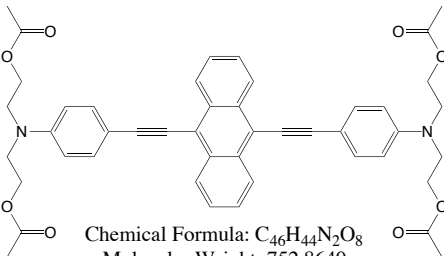
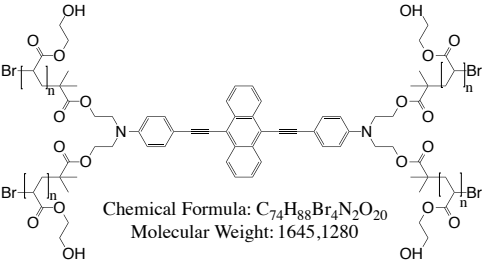
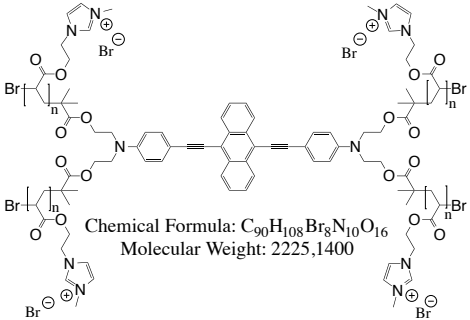
Figure 2.1: Light microscopy photographs of rat glioma (F98) in (a) and Chinese hamster ovary cells (CHO-K1) in (b). Both cell lines were used in the master thesis. [24, 25]

2.2 The chromophores

The chromophores (4 different) were synthesized by Bastien Mettra (PhD-candidate) and coworkers in the group of Cyrille Monnereau, ÉNS (École Normale Supérieure) Lyon (Appendix E). The photosensitizers were sent to Trondheim, Norway, with the postal service (protected from light) for testing at NTNU (Department of Physics and Department of Cancer Research and Molecular Medicine). The chromophores were soluble (as described in Table 2.1) for preparing of stock solutions, and stored at 4°C, -20°C or -80°C depending on waiting time before the actual experiment.

The **Ant**-chromophores consists of a highly fluorescent anthracene core, making them suitable for fluorescence imaging. While the **DBB**₂-chromophore is incorporated with a dibrominated benzene moiety making it especially suited for PDT due to its ability to produce singlet oxygen. The molecules with their respective structural formulas are presented in Table 2.1. [26]

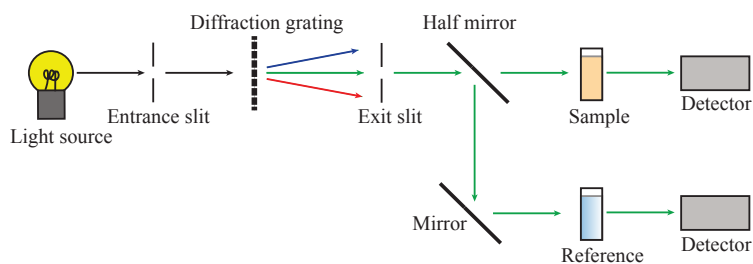
Table 2.1: Chromophores with their respective name, structural formula, chemical formula, molecular weight, and solvent. All chromophores were produced by the group of Cyrille Mannereau, ÉNS Lyon.

Name	Structural formula	Solvent for stock solutions
DBB ₂ -OAc	 <p>Chemical Formula: C₄₈H₄₀Br₄N₂O₈ Molecular Weight: 1092,4700</p>	DMSO
Ant-OAc	 <p>Chemical Formula: C₄₆H₄₄N₂O₈ Molecular Weight: 752,8640</p>	DMSO
Ant-PHEA	 <p>Chemical Formula: C₇₄H₈₈Br₄N₂O₂₀ Molecular Weight: 1645,1280</p>	dH ₂ O
Ant-PIIm	 <p>Chemical Formula: C₉₀H₁₀₈Br₈N₁₀O₁₆ Molecular Weight: 2225,1400</p>	dH ₂ O

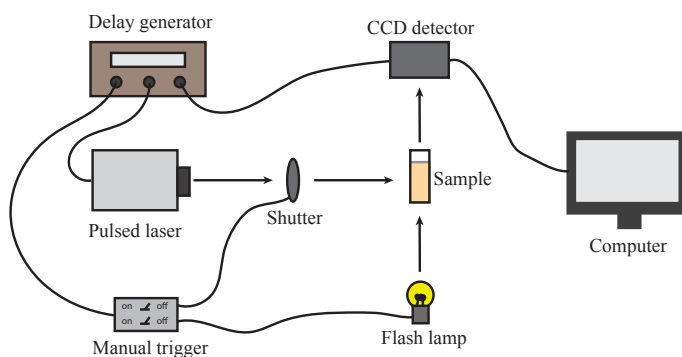
2.3 Spectroscopy

Spectroscopy is the study of matter's interaction with electromagnetic radiation. This interaction causes the matter to absorb and/or emit photons. Spectroscopy techniques are used to measure the absorption or emission of electromagnetic energy. [27]

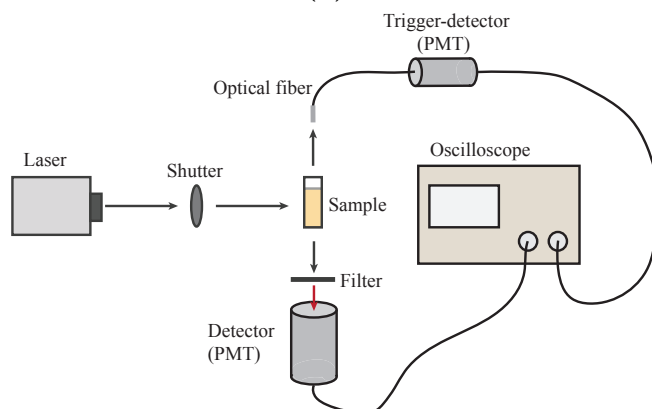
For characterization of chromophores it is most relevant to investigate absorbance, existence of excited triplet states (excited state absorption) and singlet oxygen luminescence (singlet oxygen lifetime). Basics for the relevant techniques will be summarized here, and a simplified sketch of each technique is presented in Fig. 2.2.



(a)



(b)



(c)

Figure 2.2: Simplified sketches illustrating (a) double beam absorption spectroscopy, (b) triplet excited state absorption (ESA), and (c) singlet oxygen luminescence. A filter is placed in front of the PMT (photomultiplier tube) detector in (c) such that only singlet oxygen emission (around 1270 nm) is detected.

2.3.1 Absorbance

In absorption spectroscopy, the intensity of radiation transmitted through a sample is monitored while varying the wavelength (or frequency). Beer-Lambert law, Eq. (2.1), describes the relationship between the dimensionless absorbance, A , and the intensity of the incident and emerging light, I_0 and I respectively.

$$A = \log \frac{I_0}{I} = \epsilon lc \quad (2.1)$$

Where ϵ is the molar absorption coefficient, l the path length of the radiation through the sample, and c is the concentration of the solution. [28]

The absorbance is often called *optical density* ($OD = \log(I_0/I)$), and is dimensionless. A spectrophotometer is usually used to record an absorption spectrum. In the thesis work a double-beam spectrophotometer was used. This type of spectrophotometer splits the illumination beam into two equally intense beams which are directed towards the reference- and sample channel. The outgoing signals, which correspond to I_0 and I respectively, are detected by two similar detectors. With this setup (illustrated in Fig. 2.2a), the variations in spectral and temporal intensity will affect both the reference and sample beam in the same way, and thereby minimize these effects in the resulting spectrum. [29]

During the absorption process a photon will be absorbed by the molecule (the photosensitizer (PS) in this case) causing it to be excited. Most molecules are in the lowest vibrational level at room temperature which means that the molecule during electronic excitation will end up in a vibrationally excited level of the electronic excited state as according to the Franck-Condon principle. This is illustrated in a Jablonski diagram as seen in Fig. 2.5. [30]

The Franck-Condon principle states that during an electronic transition, a change from one vibrational energy level to another is more likely to happen the more the two vibrational states (wave functions) overlap (Fig. 2.3). The principle also states that all electronic transitions occur without a change in the nuclei position. [31]

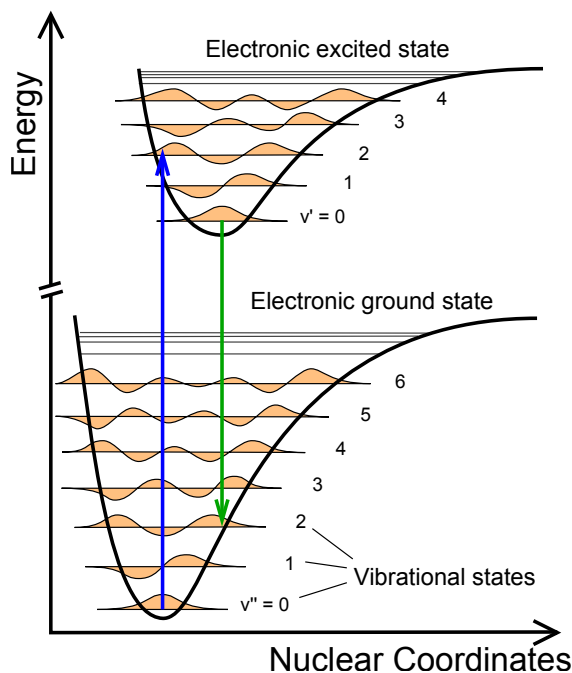


Figure 2.3: According to the Franck-Condon principle, the most probable and intense electronic transition for an excited molecule is from the ground vibrational state to the vibrational state that lies vertically above in the upper electronic state. [32, 33]

2.3.2 Luminescence

Luminescence is a collective term for *radiative decay*. Radiative decay is a process by which an electronically excited molecule lowers its excess energy by emitting a photon. The excited electron in the molecule makes a transition to a lower energy orbital, emitting a photon in the process. This is seen as a glow by an observer. There are two different types of radiative decay; *fluorescence* and *phosphorescence*. The former is decay from the molecule's excited singlet state to the singlet ground state, while the latter is decay from the excited triplet state to the singlet ground state. [32]

Fluorescence

Fluorescence is a spontaneous process. The electron in the excited orbital in the excited singlet state is paired by opposite spin to a second electron in the ground state orbital. This causes fluorescence, which is emission of a photon from a higher excited singlet state to the ground singlet state, to be spin allowed. This process is fast, and the emission rate, k_f , is typically in the order of 10^8 s^{-1} or faster. [31]

Phosphorescence

Phosphorescence is emission of a photon from the triplet state to the ground state. This transmission is spin forbidden, but the presence of several small interactions (inter- and intramolecular) makes the process weakly allowed. The process is also much slower than that for fluorescence, the emission rate, k_p , is in the range 10^6 s^{-1} to 1 s^{-1} (i.e. lifetime of 10^{-6} s to 1 s). [31, 34] The triplet state is generated by the radiationless transition intersystem crossing from the excited singlet state after the molecule has absorbed a photon. [35]

The excited singlet state, $^1\text{PS}^*$, can undergo 4 different intramolecular processes; photochemistry with rate constant k_{pc} , intersystem crossing with k_{isc} , internal conversion with k_{ic} , or fluorescence with k_f . All these processes are independent, and therefore the excited singlet state rate constant for decay is given as the following: [34]

$$k_s = k_{pc} + k_{isc} + k_{ic} + k_f. \quad (2.2)$$

The quantum yield, Φ_T , for production of the triplet state is:

$$\Phi_T = \frac{k_{isc}}{k_s}. \quad (2.3)$$

The triplet state, $^3\text{PS}^*$, can undergo three different intramolecular processes, similar to those for the excited singlet state; photochemistry with rate constant k'_{pc} , intersystem crossing with k'_{isc} , and phosphorescence with k_p . These processes are also independent. The intramolecular processes for the excited singlet state and triplet state are shown in Fig. 2.4.

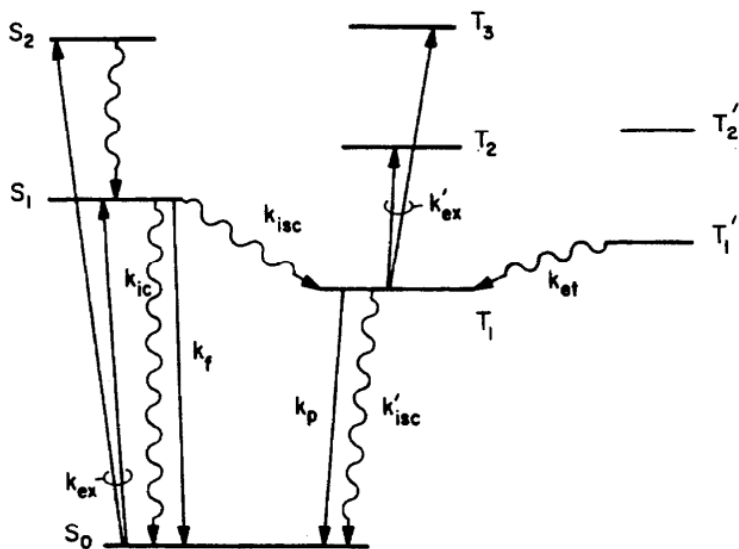


Figure 2.4: The intramolecular processes for a molecule excited to a higher singlet or triplet state. [34].

Singlet oxygen luminescence

Singlet oxygen has an extremely weak phosphorescence emission which can be detected by spectroscopic methods (Fig. 2.2c). The signal is additionally attenuated in aqueous solutions by resonance energy transfer from 1O_2 to O–H vibrations in water molecules, and by partial reabsorption of the emission signal by water. Singlet oxygen emits in the infrared region with a maximum at 1268 nm. The spectral detection of singlet oxygen luminescence is virtually free of artifacts, and gives instant results. [36]

To detect singlet oxygen luminescence the solution of interested is excited by a laser, and a PMT (photomultiplier tube) detects the signal. The detector is equipped with a filter in front which filters out other wavelengths so that only the singlet oxygen emission is detected.

Excited state absorption

Since phosphorescence usually is very weak it is difficult to assess the existence of triplet states from such measurements. Also there might be ‘dark’ photo-physical relaxation processes eventhough the state has a long lifetime. As an alternative, the triplet state can be deduced from absorbance measurements by first populating a number of triplet states from a pulsed absorption measurement. Thus, excited state absorption (ESA) is a triplet-triplet absorption process.

A method for populating and detecting the triplet state of a molecule, is to excite the molecule when it is in its ground state with irradiation within its absorption band. Then the molecule will absorb the photon, get excited to a higher singlet state, before undergoing intersystem crossing to the triplet state. [34, 37]

Only triplet ESA was measured in the thesis work (the setup is illustrated in Fig. 2.2b), but there is also possible to investigate singlet ESA. However, this technique requires much more advanced lasersystems (femtosecond pulsed lasers) due to the very short intersystem crossing time from singlet to triplet state. [38]

2.4 Photodynamic therapy

Photodynamic therapy (PDT) of cancer is a promising treatment for various solid tumors and non-malignant lesions. It is a two-step procedure which starts with adding of the photosensitizer (intravenously or topically to the patient) and activation of the drug by using non-thermal light at a specific wavelength after a given incubation time. [39]

Illumination leads to the generation of cytotoxic species in presence of oxygen, which again leads to cell death. PDT is an attractive therapy for cancer since it has high specificity and selectivity. This is due to the fact that photosensitizers after incubation will localize only in cancer tissue, because of the properties of cancer cells compared to normal cells (e.g. oxygen pressure, pH, enzym activity, and generation of new blood vessels). Only the cancer cells in illuminated areas will be treated. [1, 40]

An ideal photosensitizer for PDT should have chemical purity, high selectivity for cancer cells, minimum dark toxicity, high quantum yield of triplet state formation and a long triplet lifetime, be amphiphilic (hydrophobic to penetrate cell membranes, but also hydrophilic to disperse in bloodstream if injected intravenously), be chemical and physical stable, and have a short incubation time. It should also be activated at a wavelength which is optimal for tissue penetration, and clear from the body rapidly. Red light can penetrate further into tissue than light from other parts of the visual spectra, so photosensitizers should optimally be activated by red light. [14]

In the ground state the photosensitizer will have two electrons with opposite spins in a low energy molecular orbital, known as the singlet state. Illumination of tissue with accumulated photosensitizer will cause the photosensitizer to absorb the light in form of photons. An absorbed photon will give energy to one of the coupled electrons to move up into a higher energy orbit. The electron will keep the same spin as it had in the ground state. This excited singlet state is short lived and the electron will lose its energy by fluorescence, phosphorescence (intersystem crossing) or internal conversion into heat. The intersystem crossing is spin forbidden, but this process can be facilitated in molecules where there is spin-orbit coupling mixing the spin-levels. Especially, transition metal ions and heavy substituents, such as bromine, have such properties. The excited electron will end up in a long-lived excited triplet state with electrons with parallel spin. [14, 41] This is illustrated in a Jablonski diagram, see Fig. 2.5

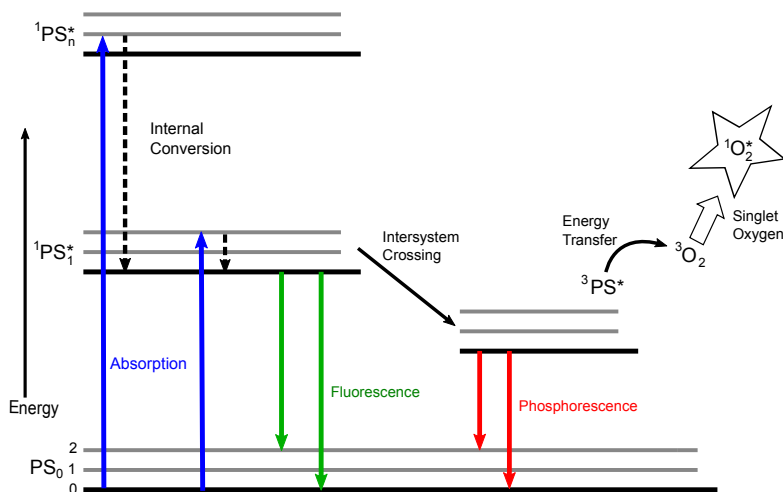


Figure 2.5: Jablonski diagram illustrating the processes a PS might undergo after absorption of a photon. Black lines illustrates electronic states, while the grey lines illustrates vibrational states. * indicates that the molecule is excited, superscript indicates if the PS is in a singlet or triplet state, and the subscript indicates the electronic state.

The excited triplet state can primarily relax to the singlet ground state giving rise to phosphorescence, or other dark' relaxation. Or it can initiate chemical reactions by undergoing two different processes. First, in a type I process, it can react with a substrate, e.g. cell membrane or molecule, and thereby transfer a proton or electron to create radical anion or cation ions: $R-OH(\equiv)$, $R-OH(-)$. These radicals might react with oxygen to produce reactive oxygen species (ROS) such as: OH^\bullet , H_2O_2 , $O_2^{\bullet-}$, etc. Secondly, in a type II process the triplet state might transfer its energy to molecular oxygen in the tissue directly. Dioxygen, O_2 , is a triplet state in its ground state, and the transferred energy converts the oxygen into excited state singlet oxygen, $^1O_2^*$, which is highly reactive. These two processes can occur at the same time, and the ratio between them is decided by the photosensitizer used, the concentration and the amount of oxygen available for the reactions (Fig. 2.6). It is generally accepted that type II is the major consequence of PDT. Both the singlet oxygen and the hydroxyl radicals have short half-lives, leading to

only molecules and structures close to the production of these will be affected by the treatment ($<0.02 \mu\text{m}$). [14, 42] Moan and Berg found that $^1\text{O}_2$ diffuse a distance of $0.01 - 0.02 \mu\text{m}$ in cells, and have a life time of $0.01 - 0.04 \mu\text{s}$ when studying the photodegradation of porphyrins in cells. [40]

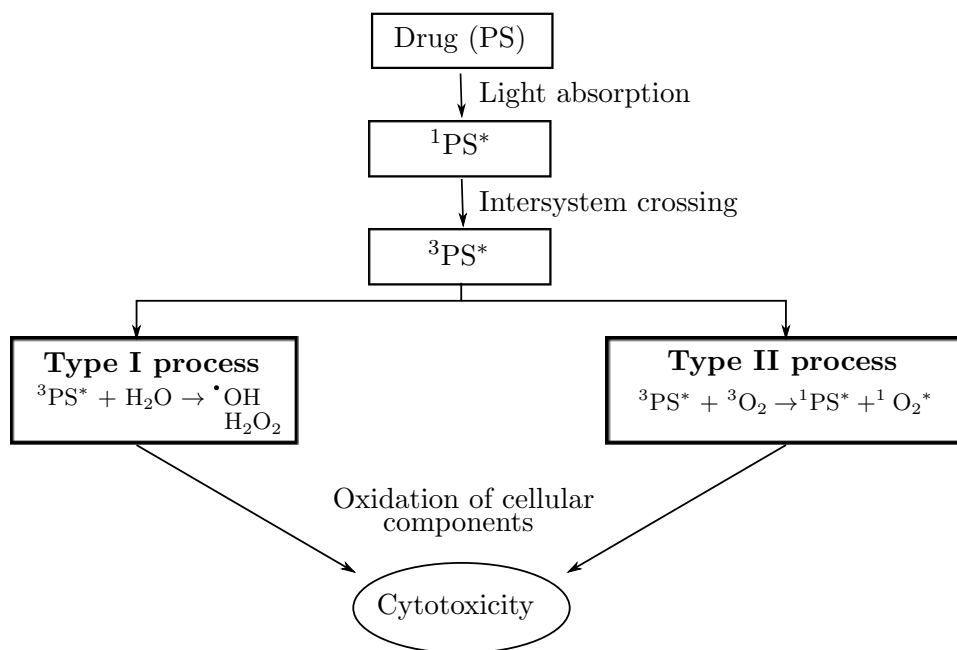


Figure 2.6: Figure showing the mechanisms for cell death following PDT. The two different processes which the triplet state can undergo are illustrated. [14]

2.5 Comet assay

There exist a number of techniques for detecting DNA damage to identify genotoxic activity in substances for example after PDT. One of the most used techniques in recent years is the comet assay, also called single-cell gel assay. The name comet describes how the cells look in a fluorescence microscope presenting DNA migration tails. The DNA migration occurs in one of the last steps of the assay during electrophoresis. [43] The ‘comets’ are scored using an inverted fluorescence microscope as described in Section 3.5

An expert panel in Washington DC in 1999 agreed on that the superior version of the assay is the one with the electrophoresis conducted under alkaline ($\text{pH} > 13$) conditions. At this pH the increased DNA migration is proportional to increased levels of direct single-strand breaks (SSB), SSB associated with incomplete excision repair sites, and alkali-labile sites (ALS). DNA is known to denaturate at $\text{pH} > 12$ due to breaking of hydrogen bonds between double strands. Also, ALS is transformed to single-strand breaks at pH-values > 12.6 . This effect is believed to be maximized at a $\text{pH} > 13$. [43]

The alkaline Comet assay was conducted as a part of the thesis work, using the cell line CHO-K1 and the chromophores Ant-PIIm and Ant-PHEA.

2.6 Confocal laser scanning microscopy

2.6.1 Theory

Thick fluorescent specimens, e.g. tissue sections and rounded cells, can cause problems when using conventional widefield optical systems due to bright fluorescent signals from areas outside the focal plane leading to increased background signal. The obtained images will have low contrast and usually overall poor quality. This problem can be solved by using confocal microscopy which rejects signals from outside the focal point by using a pinhole. [44]

A confocal microscope consist of a fluorescence microscope, a multiple laser light source, and a confocal scan head. Both a computer, monitor, and software are necessary for acquiring, processing and analyzing the images. The confocal scan head consists of different optical and electronic equipment; input from

several external laser light sources, fluorescence filter sets, a falvanometer-based raster scanning mechanism, one or more variable pinhole apertures, and a photomultiplier tube (PMT) detector.

The neglecting of information from outside the focal point is solved optically by using a focused scanning laser to illuminate the sample, and by placing a pinhole aperture in the image plane in front of the electronic photon detector. The pinhole receives fluorescence signals from the focused spot in the sample, but for most parts excludes the fluorescence signal from objects above and below the focus plane. The pinhole also excludes most of the stray light in the optical system. [44]

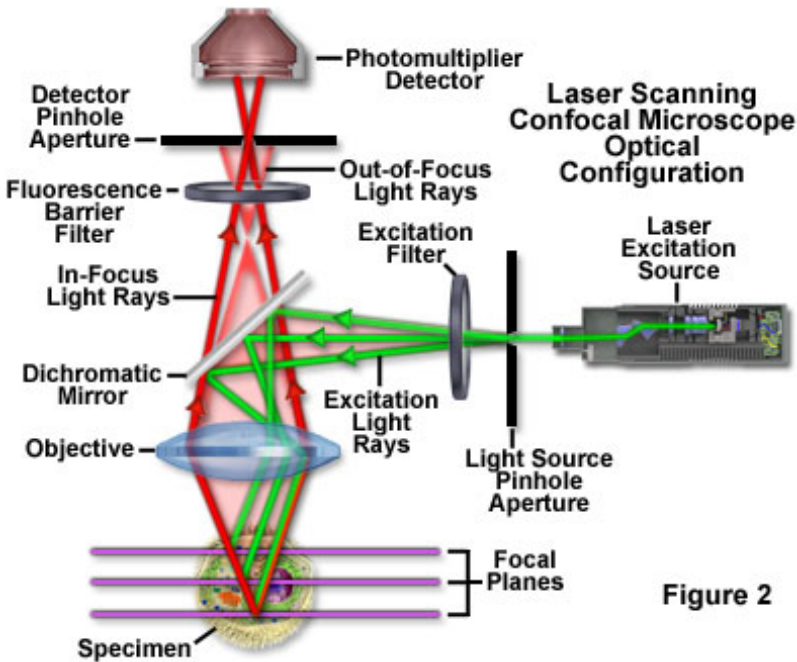


Figure 2

Figure 2.7: A schematic diagram illustrating the principle of confocal laser scanning microscopy. [45]

Epi-illumination of the sample is used in confocal microscopy, which means that the sample is illuminated from the same side as the light is detected (Fig. 2.7). This also causes the objective to function as both a condenser and an objective. The fluorescence filter set used consist of an excitation filter, emission filter, and a dichromatic mirror. The dichromatic mirror's job is to

reflect the excitation light towards the sample, while transmitting the emitted fluorescent light towards the detector.

The specimen is illuminated by scanning an intense diffraction-limited spot from side to side, and from top to bottom, hence the name confocal laser scanning microscopy.

A 3D view of the specimen can be obtained by using a stepper motor that changes the microscope's focus in very small steps along the z-axis. This enables the possibility to stack images at different z-values together to form a z-series and thereby generate a 3D view of the specimen using a computer software. [44]

The setup in confocal scanning microscopy includes a pinhole in front of the detector in a conjugate plane. The function of the pinhole is to only let light from the focal plane to get through, unwanted light from above and below the focal plane should be blocked so it does not reach the detector. This makes it possible to image a thin slice of a thick sample, where the detected light is from fluorescence. The radius of the pinhole is decided from the formula:

$$r_{airy} = \frac{0.61\lambda}{NA} \quad (2.4)$$

Where r_{airy} is the radius of the pinhole, λ is the wavelength of the excitation light, and NA is the Numerical Aperture given by the objective used. Increasing the radius of the pinhole will cause light from outside of the focal plane to be detected by the detector and thereby blur the image. Thus, the optimal setting is a trade between decrease in sensitivity and increase in resolution. [46]

2.6.2 Detecting of fluorochromes in cancer cells

The confocal microscope was a big step forward in the field of biophysical microscopy techniques when it was first introduced to the commercial market in 1987. It has many positive aspects such as the possibility to slice clean, thin optical sections out of a thick sample, view specimens in tilted planes to the line of sight, deep penetration into light scattering tissue, high resolution three-dimensional (3D) views, and the possibility to obtain differential interference- and phase-contrast images. [46]

A confocal microscope is heavily dependent on fluorescence. Fluorochromes are great to stain living cells to localize a specific structural region, to monitor dynamic processes, or to localize environmental variables. Many of the fluorescent probes are constructed in such a way that they are designed to bind with a specific biological macromolecule. [47]

Two different fluorochromes have been used along with the chromophores during confocal microscopy in the thesis work; DRAQ5 and Lysotracker Red.

DRAQ5 (Invitrogen, Eugene, Oregon, USA) is a DNA-binding anthraquinone derivative. It has enhanced DNA affinity and intracellular selectivity for DNA, which causes it to localize within the nucleus of the cell. The excitation maximum is at around 650 nm, and the fluorescence emission spectrum extends from 665 nm and beyond 780 nm. This fluorochrome is known to enter cells and nuclei rapidly, and is also suitable for two-photon excitation. [48]

Lysotracker Red (eBioscience, INC, San Diego, Ca) is a red-fluorescent dye with high selectivity of acidic organelles in living cells. It enters the cell rapidly, even at nanomolar concentrations. It has a excitation maximum at about 580 nm, and emission maximum at 590 nm. [49]

Materials and Methods

Most of the practical and experimental work performed as a part of the thesis were carried out at the Department of Cancer Research and Molecular Medicine (NTNU, Øya). With the only exception being the spectroscopy measurements of DBB₂-OAc, Ant-PHEA, and Ant-PIm, which were executed at the Department of Physics (NTNU, Gløshaugen).

3.1 Cell cultivation

The F98 cancer cell line (ATCC No. CRL-2397) is an undifferentiated malignant glioma cell line from a fetal rat brain, ordered from an ATCC catalogue (American Type Culture Collection, LGC Standards, UK) in 2012. The CHO-K1 cancer cell line (ATCC No. CCL-61) is a subclone derived from the parental CHO cell line initiated from an ovary of an adult Chinese hamster in 1957. CHO-K1 was generously supplied by Department of Cancer Research and Molecular Medicine at the Gastro Building, NTNU.

Both F98 rat glioma cells and Chinese hamster CHO-K1 ovary cells were seeded out in 10 ml growth medium (Appendices A.1 and A.2) in 75 cm² cultivation flasks, and incubated in a standard cell incubator (37°C) with 95% humidified atmosphere and 5% CO₂. The cells were split twice a week.

3.2 The chromophores

Chromophores were stored in the following way:

- Pure powder (ampoules from Lyon): -80°C
- Stock solution: -80°C
- Working solution (short periods): -20°C

3.3 MTT assay

MTT assay is a well used method to measure the number of living cells after a cytotoxic treatment *in vitro* such as PDT. The yellow tetrazolium salt MTT, or 3-(4,5-dimethylthiazol-2-yl)-2,5-diphenyl tetrazolium bromide, converts into purple formazan crystals by living cells, and determines mitochondrial activities in viable cells. The number of cells is linearly related to the amount of formazan crystals created, and thereby the shade of purple of the samples (mitochondrial activity is constant for most cells). [50, 51]

The MTT formazan reaction product is only partially soluble in the medium, and of that reason an alcohol were used dissolving the formazan crystals producing a homogenous solution. In the present study isopropanol were used as solvent, and the absorption ($\lambda_{ex} = 595 \text{ nm}$) were performed by a double beam spectrophotometer. [52]

3.4 PDT-experiment

The concentration of the photosensitizers were chosen on basis of results from previous pilot experiments in collaboration with Odrun Gederaas.

3.4.1 Light source

A PCI Biotech LumiSource lamp (Oslo, Norway) with continous light delivery at $\lambda = 435 \text{ nm}$ and fluence rate of 12.9 mW/cm^2 was used for light illumination as part of PDT-experiments. More information in Appendix G.

3.4.2 Cell survival study - Experimental procedure of MTT assay

Day 1

The cells were washed with PBS, harvested from 75 cm² cultivation flasks and loosened from the bottom by using the enzyme Trypsin. Growth medium (10 ml) were added to the cells in Trypsin in a 50 ml tube, and centrifugated (5 min, 1500 rpm, 4°C) removing dead cells. The supernatant was removed, leaving the cell pellet before resuspended in growth medium (500 µl). The cell suspension was further diluted with growth medium to a total volume of 10 ml.

Twenty µl of the cell suspension was added to a Bürker chamber. The cell number in four 1 mm² squares were counted to find the cell concentration in the stock solution (Appendix F).

After dilution with growth medium, the cells were seeded out in petri dishes (diameter=60 mm) containing 3 ml suspension ($0.25 - 0.35 \cdot 10^6$ cells/dish). The dishes were incubated for ~24 h in 37°C, and each experiment contained 20 – 30 dishes.

Day 2

Growth medium was removed and new added (3 ml, 37°C) to control dishes without photosensitizer incubation. Growth medium was removed, and photosensitizer-enriched medium (3 ml, 37°C) were added to the remaining dishes in the dark. All dishes were covered with aluminium foil and incubated for 24 h (37°C, 5% CO₂).

Day 3

After washing two times with PBS (3 ml, 37°C), growth medium (3 ml, 37°C) were added to control dishes without light treatment, before placing in incubator (37°C, 5% CO₂). Further, PBS were added (3 ml, 37°C) to all the remaining dishes before monochromatic blue light illumination (435 nm, 12.9 mW/cm²) as the standard in the master thesis (Section 3.4.1). After light treatment with the respective time intervals, the PBS were removed, and growth medium added (3 ml, 37°C) before further incubation (24 h, 37°C).



Figure 3.1: LumiSource lamp (PCI Biotech, Oslo, Norway) used for blue light PDT. The lamp illuminates with monochromatic light of wavelength $\lambda = 435$ nm (Section 3.4.1). This photo shows petri dishes with adherent cells placed on top of the lamp before treatment. The illumination periods (min) were described by red numbers on top of the dish.

Day 4

The MTT assay (Section 3.3) was performed 24 h after PDT treatment measuring the number of living cells.

MTT working solution (0.5 mg/ml) was made fresh using 1 part MTT stock solution (5 mg/ml, 37°C) and 9 parts growth medium (37°C). All dishes were carefully washed with PBS (3 ml, RT), before adding the MTT working solution (2 ml, 1 h, 37°C).

After incubation the MTT working solution was removed, and isopropanol (2 ml, RT) added before placing on an orbital shaker (30 min, 80 rpm). The isopropanol and cell suspensions were transferred into 15 ml tubes, and centrifugated (5 min, 1500 rpm, 4°C).



Figure 3.2: Cell suspension in numbered 15 ml tubes as part of MTT assay subsequent light treatment (24 h).

The supernatant (1.0 ml) was transferred into cuvettes, and if necessary diluted 10 times with isopropanol. The absorbance were measured using a double beam UV-Vis Spectrophotometer UV-1700 (Shimadzu, Japan), using isopropanol as refrence at the excitation wavelength $\lambda_{ex} = 595$ nm.

3.5 Comet assay

According to litterature, the alkaline ($\text{pH} > 13$) version of the Comet assay was found to be the optimal version by an expert panel at International Workshop on Genotoxicity Test Procedures (IWGTP), Washington DC, 1999. [43] This version is used in the master thesis.

3.5.1 Experimental procedure

Day 1

The first steps of the cell seeding process were identical to those for PDT-experiment, and are described in Section 3.4.

Cells were seeded out in six-well cell culture plates, with a 3 ml cell suspension containing 100,000 cells in each well. Cells were incubated for 24 h in 37°C .

Day 2

Conventional microscope slides were added agarose gel in two steps. First, the slides were prepared by dipping in methanol before burning over a blue flame (to be cleaned for oil and dust). Then the slides were dipped in normal

melting agarose gel (1%), and the backside was wiped off before drying over night (50°C) (Appendix B.1).

The cells were incubated with Ant-PIIm (2.5 μ M or 10 μ M, 2 ml, 24h, 37°C, 5% CO₂) or Ant-PHEA (2.5 μ M, 2 ml, 24 h, 37°C, 5% CO₂).

Day 3

The cells were treated with monochromatic blue light (435 nm, 12.9 mW/cm²) as the standard illumination in the master thesis (Section 3.4.1), and harvested posttreatment. After suspended in low melting agarose gel (1%), the cell suspension (75 μ l) were put on ice with a coverslip in duplicates (Appendix B.2). The coverslip was removed after a few minutes before placing of slides in glass jar containing lysis solution (4°C, 24 – 48 h) (Appendix B.3).

Day 4

The following steps were performed in 4°C: The slides were washed with alkali electrophoresis buffer (pH > 13) twice before incubation in same buffer (30 min), which also were used during the electrophoresis (Appendix B.4). The electrophoretic conditions were 20 V and 300 mA. The DNA-enriched samples were electrophoresed for 25 min, and the slides were neutralized in a neutralizing buffer (10 min) before rinsed with dH₂O (Appendix B.5). At the end the slides were dried (15 min, 50°C), before being stored in the dark at RT until comet scoring (dried slides can be stored for a long time before counting).

The fluorescent dye EtBr (ethidium bromide) was added (25 μ l, 15 μ g/ml) on top of the slides immediately before comet scoring using an invert fluorescent microscope (Zeiss Axiovert 200M, Germany) with a RHOD filter (535 – 585 nm) connected to a Sony XCD-X700 camera. The imaging software *Kinetic Komet 5.5* (Andor Technology, United Kingdom) was used to pick and evaluate 100 comets randomly.

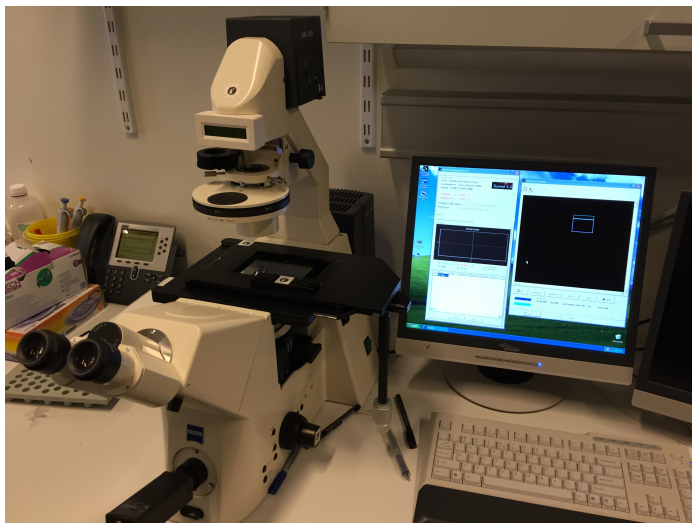


Figure 3.3: Invert fluorescent microscope (Zeiss Axiovert 200M, Germany) equipped with a Sony XCD-X700 camera used for comet scoring in the comet assay.

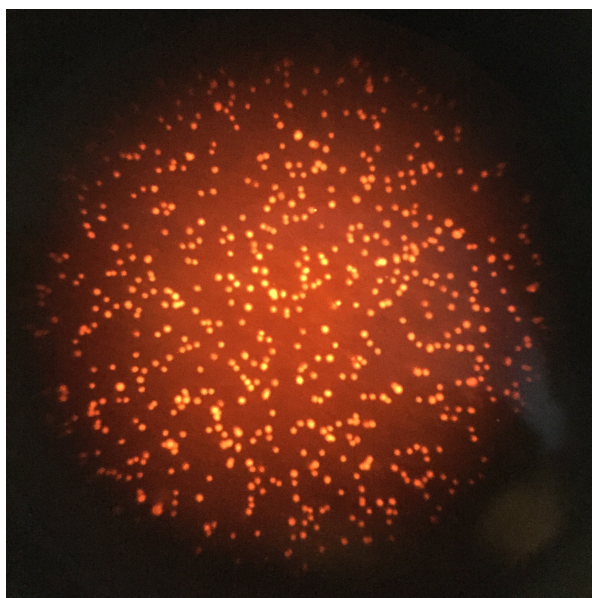


Figure 3.4: Photograph of CHO-K1 cells taken through the bioculars of the fluorescence microscope used for the Comet assay. A 10x objective and a HBO 100 light source with a RHOD filter was used for illumination, and EtBr for staining of comets.

3.6 Confocal laser scanning microscopy

3.6.1 Experimental procedure

Day 1

The first steps of the cell seeding process were identical to those for PDT-experiment, and are described in Section 3.4.

For confocal laser scanning microscopy glass bottom microwell dishes (diameter=35 mm) were used, with a 2 ml cell suspension containing 300,000 cells in each dish. Cells were incubated for 24 h in 37°C.

Day 2

Growth medium was removed and new added (2 ml, 37°C) to control dishes without chromophore incubation. Growth medium was removed, and the respective chromophores (2 ml, 37°C) were added to remaining dishes in the dark. All dishes were covered with aluminium foil before incubation (24 h, 37°C, 5% CO₂).

Day 3

Before adding growth medium (2 ml, 37°C), the dishes were washed two times with PBS (2 ml, RT) before examining under the confocal microscope.

For DNA staining the dishes were added DRAQ5 (1 µM, 1 ml, 15 min, 37°C, 5% CO₂) and studied under the confocal microscope in the DRAQ5/growth medium solution (Section 2.6.2).

For lysosome staining the dishes were added LysoTracker Red (50 nM, 1 ml, 1 h, 37°C, 5% CO₂), and later incubated with growth medium (2 ml, 30 min, 37°C, 5% CO₂) before examination under the confocal microscope (Section 2.6.2).

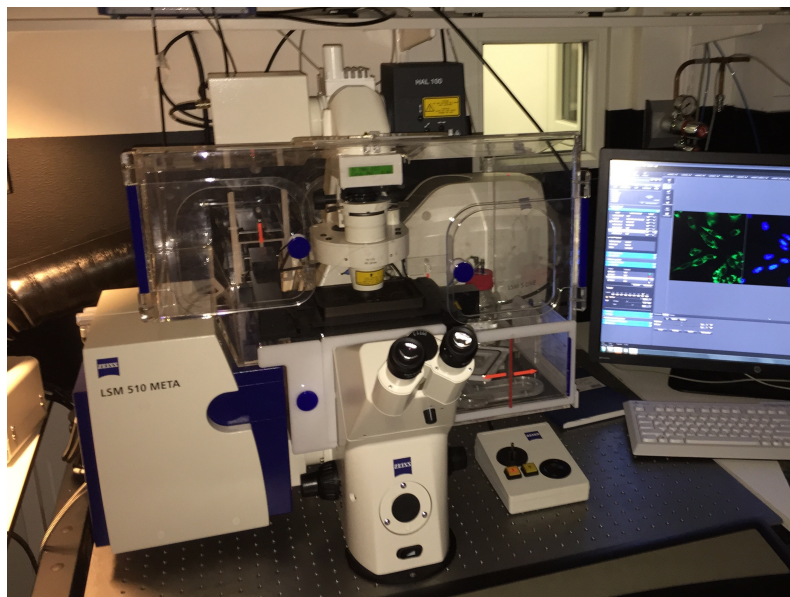


Figure 3.5: Laser scanning confocal microscope (Zeiss LSM 5 DUO, Zeiss 510 META, Zeiss LSM 5 Live, Germany) at the Gastro Centre, NTNU/St. Olav Hospital.

3.7 Spectroscopy

The simplified techniques for absorbance, excited state absorbance, and singlet oxygen luminescence are illustrated in Fig. 2.2.

3.7.1 Absorbance

The absorbance spectra were obtained using an UV-1601PC UV-Visible scanning spectrophotometer (Shimadzu, Japan), and the software UVProbe 1.11 (Shimadzu, Japan).

3.7.2 Excited state absorbance

The excited state absorbances were measured using a NT 342B-SH-10-WW laser (Ekspla, Lithuania), monochromator (Applied Photophysics, United Kingdom), and 150 W Xenon lamp with BWSpec software (B&W Tek, USA).

The chromophore solutions (3 ml, RT) were added in quartz cuvettes (10

mm). Air was removed from samples either by purging with Argon gas for approximately 5 min, or by using a vacuum system and a series of at least 3 freeze-thaw cycles with liquid nitrogen.

3.7.3 Transient state lifetime

The transient state lifetime was measured using the same setup as for excited state absorbance just with an increasing delay between excitation and detection of the emitted signal. The delay was set in microseconds and shows how the phosphorescence signal decay over time.

Samples were prepared the same way as for ESA.

3.7.4 Singlet oxygen lifetime

The singlet oxygen lifetime was measured using a NT 342B-SH-10-WW laser (Ekspla, Lithuania), and an Infiniium 54830BDSU oscilloscope (Keysight, United States).

The chromophore solutions (3 ml, RT) were added in quartz cuvettes (10 mm). To obtain a reference signal, air was removed from samples in same way as described in Section 3.7.2. A filter is placed in front of the PMT detector such that only singlet oxygen emission (around 1270 nm) is detected (Fig. 2.2).

Chapter 4

Results

4.1 Cell death following PDT with continuous light delivery

The first PDT-experiment with a subsequent MTT assay was carried out for the chromophore Ant-PIIm (December 2014) with CHO-K1 cells, and repeated later (January 2015). All samples were conducted in duplicates. One experiment with just light-only treated cells was conducted (February 2015) due to unexpected and strange results for these samples in the January experiment (Fig. 4.1). The data point for ‘Light’ at 20 min (Fig. 4.1) is only based on one sample due to a not representative result for one of the dishes at this point. The PCI Biotech LumiSource (12.9 mW/cm²) lamp with continuous light delivery at $\lambda = 435$ nm was used for all the experiments (Section 3.4.1).

The mean lethal dose, LD₅₀, is reached already before 1 min of illumination (435 nm, 12.9 mW/cm²) in Ant-PIIm incubated (10 μ M, 24 h, 37°C, 5% CO₂) CHO-K1 cells as shown in Fig. 4.1. During the next two minutes the cell survival is more or less stable (36 – 38%) before further decrease until partly complete cell death (98%) after 20 minutes illumination.

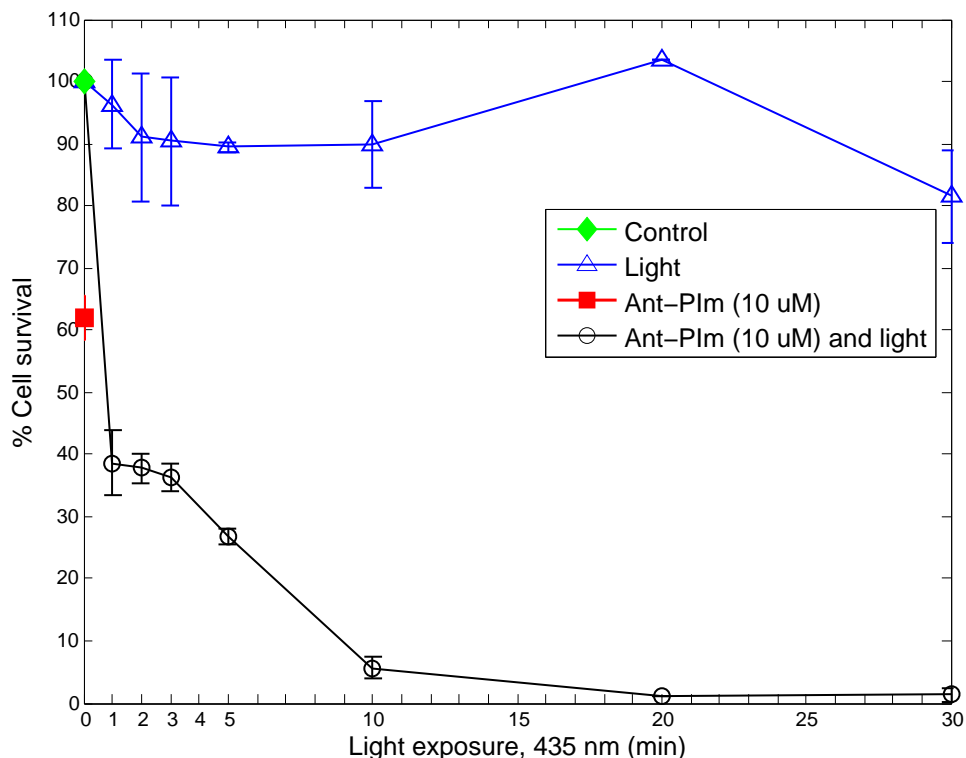


Figure 4.1: Cell survival curve for CHO-K1 cell line after PDT using Ant-PIIm (10 μ M), based on two individually experiments with controls in triplicates, and the rest in duplicates. The data point for ‘Light’ at 20 min is only based on one sample, since one of the two dishes gave an unreasonable high result for cell survival and is hence disregarded.

The curve for cells only treated with light in Fig. 4.1 is based on an independent experiment conducted with only these samples, which is not standard procedure. This experiment led to a survival curve for light-only treated cells which was as expected (little cell death), but not representative since it was not a part the experiments where Ant-PIIm or Ant-PHEA were included and differed from light-only cell survival curves obtained in the other experiments (Fig. 5.1).

The chromophore Ant-PHEA was tested in two different PDT experiments (April 2015) with CHO-K1 cells; first with a concentration of 10 μ M in dupli-

ates together with a few samples of Ant-PIm (10 μM) just to check that same results were achieved as for previous experiments with Ant-PIm. In the second experiment, Ant-PHEA was tested with three different concentrations; 10 μM , 50 μM , and 100 μM , all in singles. The results for Ant-PHEA are presented in Fig. 4.2.

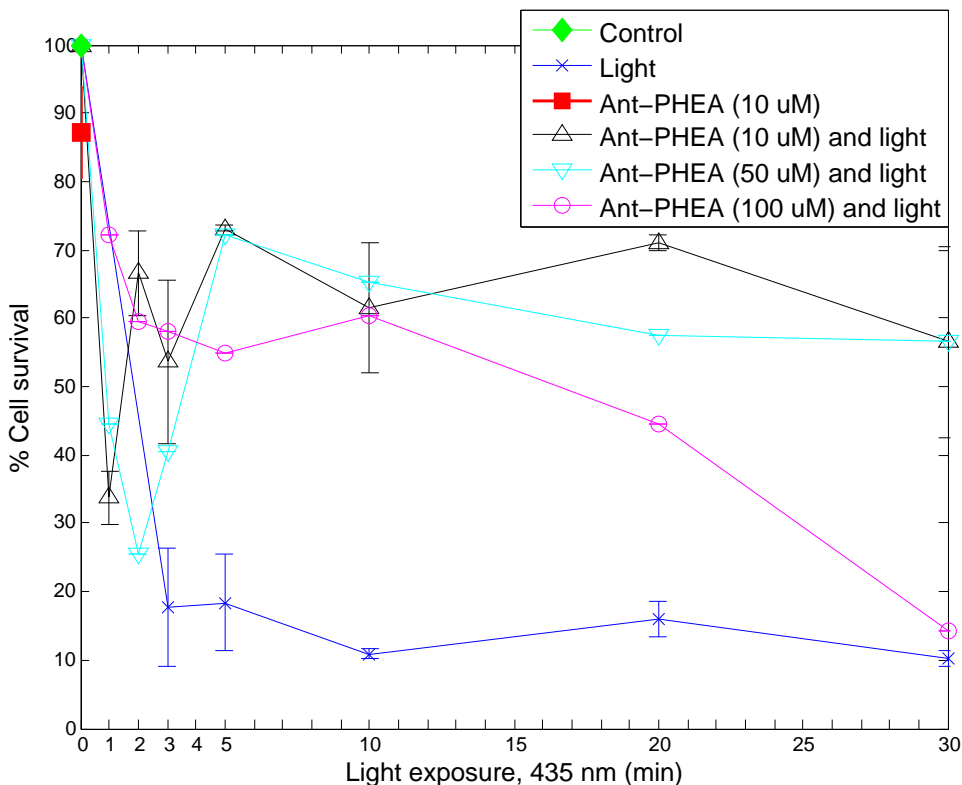


Figure 4.2: Cell survival curve for CHO-K1 cell line after PDT-treatment with different concentrations of Ant-PHEA (10 μM , 50 μM , 100 μM). All data are based on results from two experiments, some as single samples (50 μM and light, 100 μM and light), duplicates (light, 10 μM , 10 μM and light), and triplicates (controls). The dark toxicity (chromophore incubation, but no illumination) was not measured for Ant-PHEA of 50 μM and 100 μM .

For the 10 μM and 50 μM Ant-PHEA incubated cells an evident decrease was observed after both 1, 2 and 3 min of light. There is an increase in cell survival to over 70% after 5 min of illumination, and after 30 min there is about 60% cells alive.

The survival curve of light-only treated cells in Fig. 4.2 shows significant cell death.

The Ant-PHEA chromophore has an evident less dark toxicity effect compared to Ant-PIm with as little as 10% cell death from the chromophore alone compared to almost 40% for Ant-PIm (Figs. 4.1 and 4.2).

4.2 Comet assay after Ant-PIm and Ant-PHEA induced PDT

The comet assay was conducted in collaboration with co-supervisor Odrun Gederaas (February 2015) and the first experiment led to only three readable samples (not included here). It was further repeated (April 2015) investigating Ant-PIm (2.5 μM) and Ant-PHEA (2.5 μM) in combination with light treatment (435 nm, 12.9 mW/cm^2 , 30 sec) in CHO-K1 cells. The counting of comets and data analysis was performed by the master student, and the results are plotted in Fig. 4.3.

The indirect DNA damage are presented in Fig. 4.3. There are no significant difference among the control (untreated cells), light-only, drug-only, and PDT samples, which indicates no DNA damage caused by light, drug, or light-drug combinations.

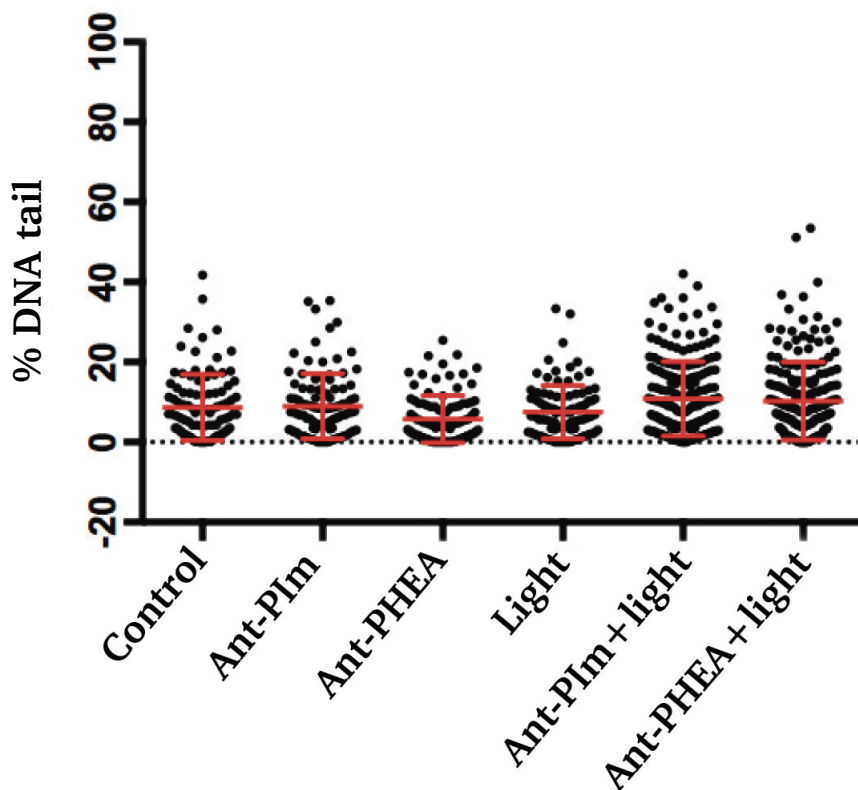


Figure 4.3: Distribution of comet tails (%) based on two individual experiments of CHO-K1 cells: untreated cells (controls), drug-only (Ant-PIm and Ant-PHEA) treated cells, light-only treated cells, Ant-PIm-PDT-treated cells, and Ant-PHEA-PDT-treated cells, with the mean comet tail movement \pm SD (in red) for each sample. A concentration of 2.5 μ M was used for both drugs (24 h, 37°C, 5% CO₂), and blue light (435 nm, 12.9 mW/cm²) for illumination. All samples were harvested straight after treatment.

4.3 Spectroscopy

4.3.1 Absorbance

The absorbance spectra of DBB₂-OAc, Ant-PIIm and Ant-PHEA, all with dH₂O as solvent, are presented in Fig. 4.4. The chromophores' spectra were not recorded for the same concentration.

The absorbance spectrum for Ant-PIIm recorded twice, while the ones for DBB₂-OAc and Ant-PHEA were recorded once. The spectra for Ant-PIIm were identical both times, and only one is presented here (Fig. 4.4).

Ant-PIIm and Ant-PHEA seems to have almost identical spectra, while the one for DBB₂-OAc differ from the two others.

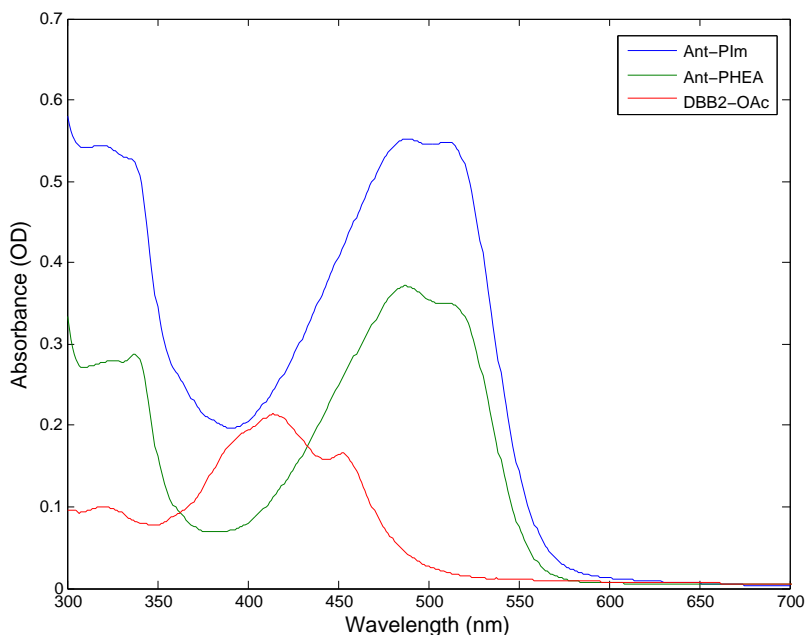


Figure 4.4: Absorbance spectra of Ant-PIIm in blue (January 2015), Ant-PHEA in green (April 2015), and DBB₂-OAc in red (March 2015). All spectra were recorded with dH₂O as reference.

4.3.2 Excited state absorbance

When measuring the excited state absorbance one needs to record several reference signals. Firstly, a ‘dark’ spectrum must be recorded (only the laser signal). Secondly, the ‘reference’ spectrum is collected (only the flash lamp). At last, the signal from the sample together with both excitations is recorded. The absorbance signal given by the software was then corrected for fluorescence and the dark baseline adjusted according to the following formula:

$$A = \log \left(\frac{I_{\text{ref}} - I_{\text{dark},0}}{I_{\text{sample}} - I_{\text{dark},1}} \right), \quad (4.1)$$

where I_{ref} is the reference-signal, $I_{\text{dark},0}$ is the average of the dark-signal $I_{\text{dark},1}$ with the fluorescence part cut out, and I_{sample} is the raw data-signal from the sample with both excitations.

The excited state absorbance (ESA) performed for DBB₂-OAc (50 μM) in a mixture of dH₂O and THF (October 2014) is presented in Fig. 4.5. The ESA spectrum was only recorded once for this chromophore.

Initially the excited state absorbance for Ant-PIm (17 μM) in dH₂O was performed (January 2015), and later repeated (March 2015). The same poor signal was achieved both times, so only the first results from January 2015 are presented (Fig. 4.6). The excitation radiation wavelength varied between 425 and 500 nm, and the average was made from signals after correcting for fluorescence. The signal shows little variation in strength for the different excitation wavelengths applied.

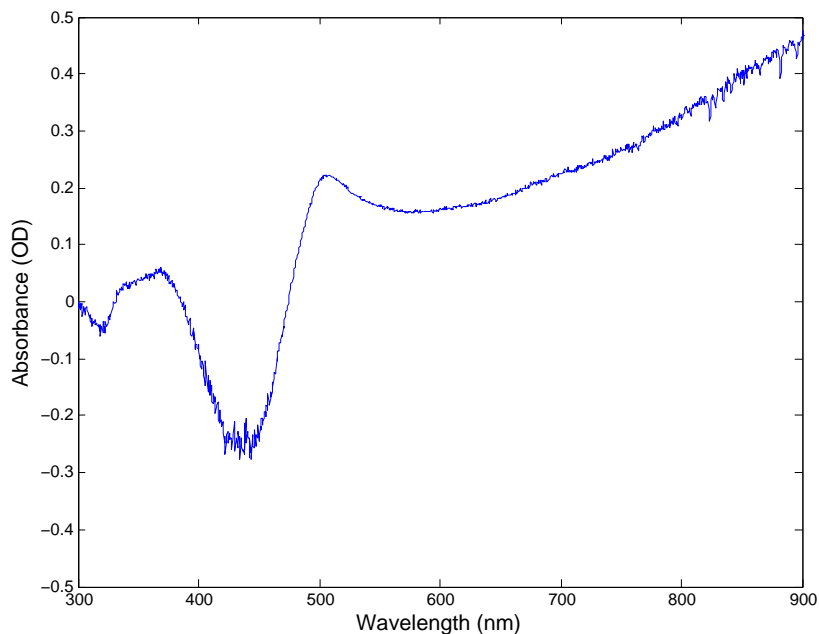


Figure 4.5: Excited state absorbance spectrum for triplet state of DBB₂-OAc (50 μ M) in a mixture of dH₂O and THF (October 2014). The signal is corrected for fluorescence.

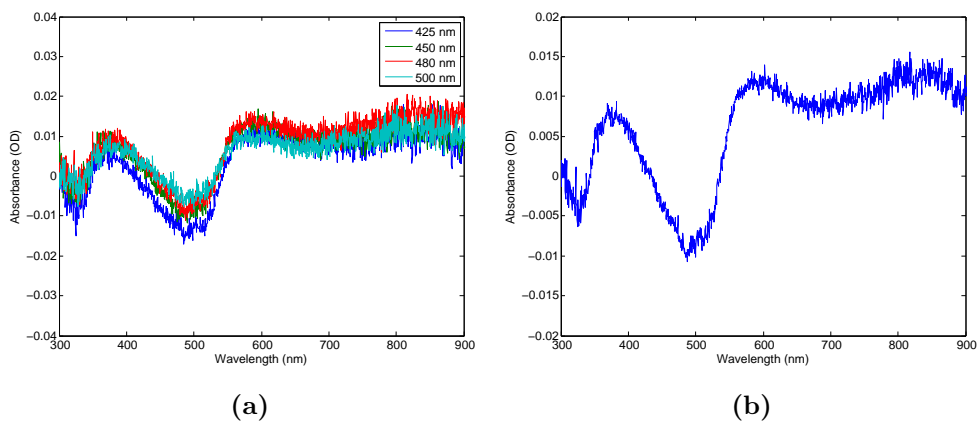


Figure 4.6: Excited state absorption of Ant-PIm (17 μ M) in dH₂O (January 2015) with excitation radiation varying between 425 and 500 nm after correction for fluorescence is presented in (a). The average of all 4 signals is shown in (b).

The ESA for Ant-PHEA ($9\ \mu\text{M}$) in dH_2O was obtained in April 2015 (Fig. 4.7). The excitation radiation wavelength was varied between 430 and 520 nm, and an average was made from the signals after correcting for fluorescence. The ESA spectrum was only recorded once for this chromophore.

The signals spread distinctly beyond $\sim 550\ \text{nm}$.

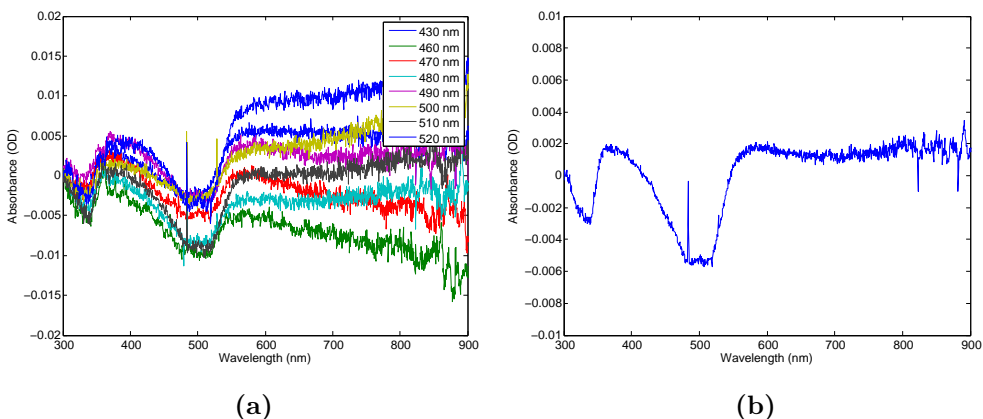


Figure 4.7: Excited state absorption of Ant-PHEA ($9\ \mu\text{M}$) in dH_2O (April 2015) with excitation radiation varying between 430 and 520 nm after correction for fluorescence is presented in **(a)**. The average of all 8 signals is shown in **(b)**. The ‘spike’ (recorded at $\sim 480\ \text{nm}$) is from the laser.

The average signals for $\text{DBB}_2\text{-OAc}$, Ant-PIm and Ant-PHEA are plotted in Fig. 4.8 for comparison. The signal for $\text{DBB}_2\text{-OAc}$ is clearly stronger than the signal for Ant-PIm and Ant-PHEA which is rather poor (Fig. 4.8a). This is partly due to a higher concentration of $\text{DBB}_2\text{-OAc}$ compared to Ant-PIm and Ant-PHEA. The signal for Ant-PIm is similar in shape to the signal for Ant-PHEA, but also stronger (Fig. 4.8b). The concentration of Ant-PHEA solution used in this experiment was lower than the one for Ant-PIm, which is also why the signal is weaker for Ant-PIm.

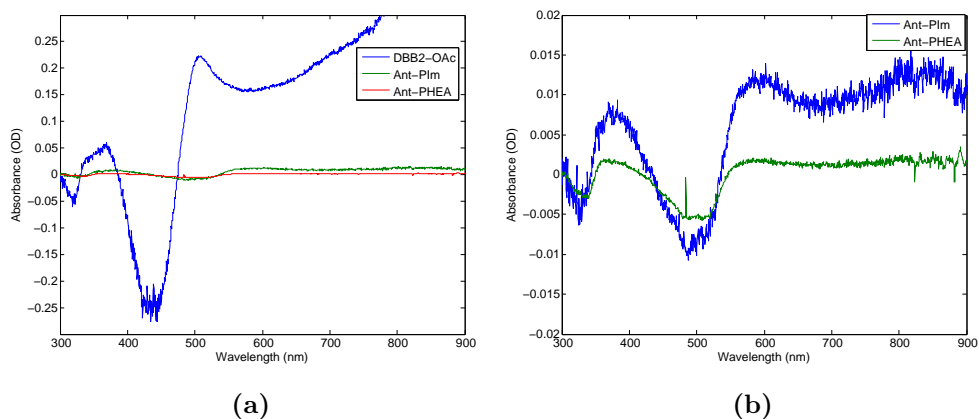


Figure 4.8: Excited state absorptions of DBB₂-OAc (50 μ M) in a mixture of dH₂O and THF, Ant-PIm (17 μ M) in dH₂O, and Ant-PHEA (9 μ M) in dH₂O after correction for fluorescence are presented in (a). Excited state absorptions of Ant-PIm in dH₂O, and Ant-PHEA in dH₂O after correction for fluorescence are shown in (b). The ‘spike’ (recorded at \sim 480 nm) is from the laser.

4.3.3 Transient state lifetime

The transient state lifetime was examined for DBB₂-OAc (Fig. 4.9b) by measuring the spectra between excitation of triplet state and detection of resulting signals. The absorbance for the given wavelength, as a function of time, was plotted to find the transient state lifetime (Fig. 4.9). This experiment was conducted once.

DBB₂-OAc was the only chromophore with a strong enough ESA signal for calculation of transient state lifetime.

Figure 4.9a illustrates signal strength decay with increasing time delay (μ s) between excitation and detection, while Fig. 4.9b shows how the signal decays, and that the lifetime is in order of 10^{-4} s. This is a relatively fast decay, and in the range of the triplet state lifetime which is in general 10^{-6} s to 1 s. [31, 34]

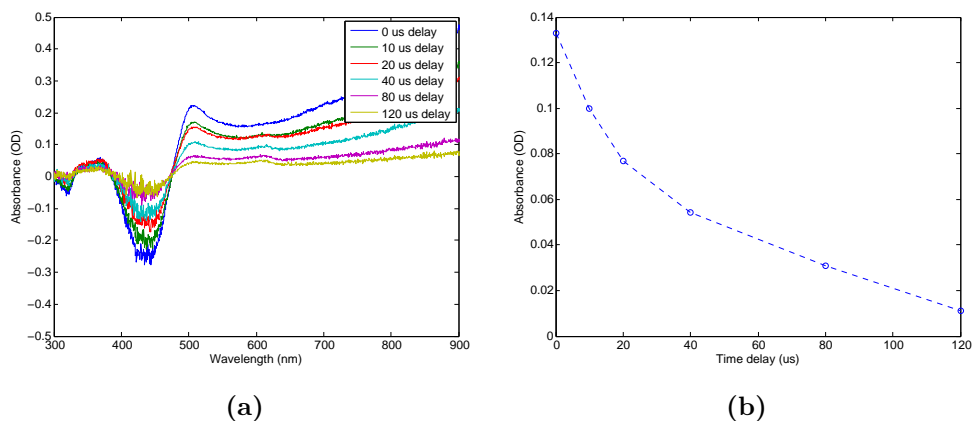


Figure 4.9: The excited state absorption signal of DBB₂-OAc with increasing time delay is presented in (a). The transient state lifetime (μs) of DBB₂-OAc based on absorbance for the given wavelength from all the signals is shown in (b).

4.3.4 Singlet oxygen lifetime

The singlet oxygen lifetime was investigated for DBB₂-OAc and Ant-PIm; once for DBB₂-OAc, and twice for Ant-PIm (similar results were achieved both times with the last being presented here). The signal detected for DBB₂-OAc is more evident than the signal detected for Ant-PIm (Figs. 4.10a and 4.11a)

The singlet oxygen detected for the Ant-PIm solution with air are higher compared to signals from the sample without air (more signal > 0 compared to signal < 0), although this difference is almost negligible (Fig. 4.11). While the difference is more apparent for the DBB₂-OAc solution (Fig. 4.10).

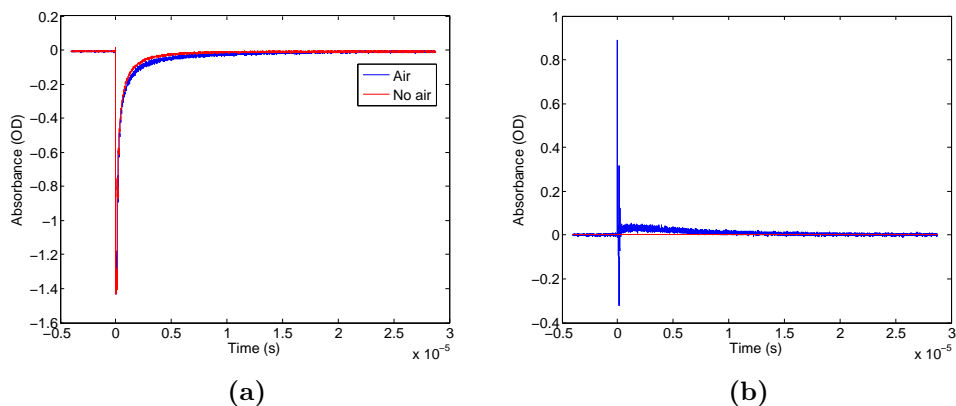


Figure 4.10: The singlet oxygen lifetime (s) for DBB₂-OAc (50 μ M) in a mixture of dH₂O and THF, recorded (64 averages) for sample with/without air (removed by Argon gas) is presented in (a). A plot of the singlet oxygen lifetime (s) with air subtracted from the singlet oxygen lifetime without air is shown in (b).

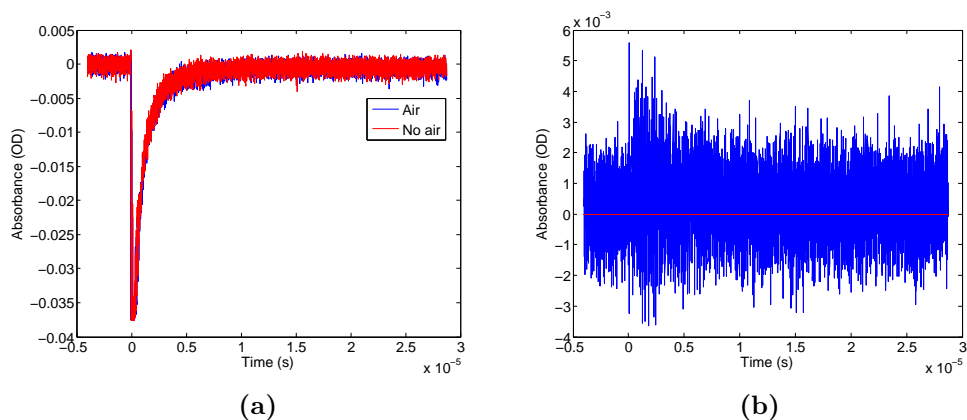


Figure 4.11: The singlet oxygen lifetime (s) for Ant-PIIm (25 μ M) in dH₂O, recorded (128 averages) for sample with/without air (removed by Argon gas) is presented in (a). A plot of the singlet oxygen lifetime (s) with air subtracted from the singlet oxygen lifetime without air is shown in (b).

4.4 Localization of chromophores in F98 rat glioma cells

The localization of 3 different chromophores (synthesized at ÉNS Lyon) (Table 2.1) in F98 glioma cells were investigated using a confocal laser scanning microscope (Zeiss LSM 5 Duo, Zeiss LSM 510 META, Zeiss LSM 5 Live, Germany) (Fig. 3.5). The investigated chromophores were Ant-PHEA, and Ant-OAc (5 μM , 3 ml, 24 h, 37°C, 5% CO_2), as well as $\text{DBB}_2\text{-OAc}$ (10 μM , 3 ml, 24 h, 37°C, 5% CO_2). Markers for confocal microscopy were added for detection of cell components, described in Section 2.6.2. The marker for DNA was DRAQ5 (1 μM , 2 ml, 15 min, 37°C, 5% CO_2), and for lysosomes LysoTracker Red (50 nM, 1 h, 37°C, 5% CO_2).

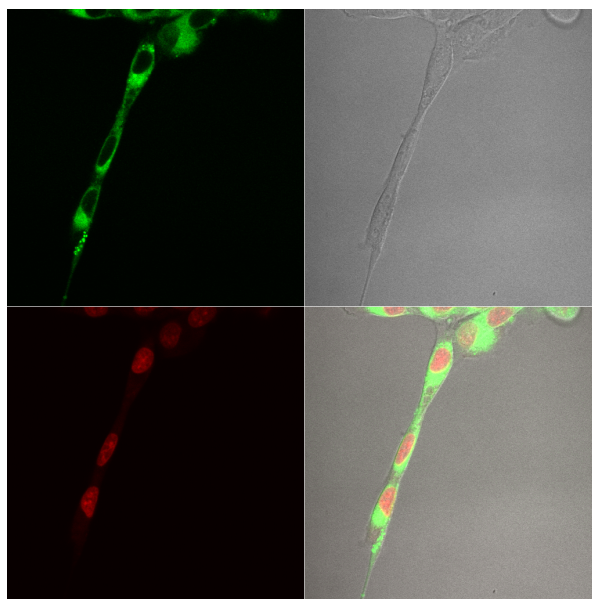
The confocal microscopy was performed using a Plan-Apochromate 63x/1.4 oil DIC objective, and the live cell images acquired in growth medium (37°C). One channel was used for chromophores with an Argon/2 laser (488 nm), and another channel for fluorescence markers (DRAQ5 and LysoTracker Red) with a HeNe laser (633 nm).

The confocal image of Ant-OAc (5 μM , 3 ml, 24 h, 37°C, 5% CO_2) with the DNA marker DRAQ5 are shown in Fig. 4.12a. Cells incubated with Ant-OAc after staining with LysoTracker Red are presented in Fig. 4.12b. The images (Fig. 4.12) documents the localition of Ant-OAc in cytoplasmic vesicles which seems to correspond to the lysosomes, and not in the nucleus.

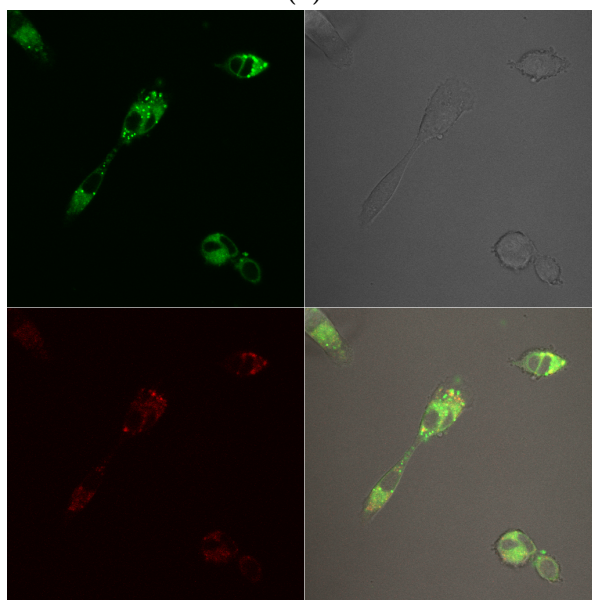
The confocal images of Ant-PHEA (5 μM , 3 ml, 24 h, 37°C, 5% CO_2) with DNA and lysosome staining are presented in Fig. 4.13. The images (Fig. 4.13) documents the localition of Ant-OAc in cytoplasmic vesicles which seems to correspond to the lysosomes, and not in the nucleus.

The confocal image of $\text{DBB}_2\text{-OAc}$ (10 μM , 3 ml, 24 h, 37°C, 5% CO_2) with DNA and lysosome staining are presented in Fig. 4.14. The figures suggest that $\text{DBB}_2\text{-OAc}$ might not be completely dissolved. Figure 4.14b documents the localition of Ant-OAc in cytoplasmic vesicles which might correspond to the lysosomes, and not in the nucleus. The fluorescence signal was overall poorly for this chromophore. A concentration of 5 μM was originally used (images not shown here), but increased the next day due too weak fluroescence signal.

Ant-OAc and Ant-PHEA are localized outside the cell nucleus in F98, and seem to be localized in the lysosomes detected by Lysotracker Red. This hypothesis is supported by Figs. C.1-C.4 which illustrates the colocalization of Ant-OAc and Ant-PHEA with Lysotracker Red, and very little with DRAQ5. Table 4.1 presents similarly high values of the colocalization factor, C_f (defined in Eq. (4.2)), for both chromophores using Lysotracker Red ($\sim 40\%$ in F98 cells), and DRAQ5 ($1 - 5\%$ in F98 cells). DBB₂-OAc fluorescence weakly and was therefore hard to localize. However, Fig. 4.14b along with the C_f -value for DBB₂-OAc with Lysotracker Red documents some colocalization in lysosomes.

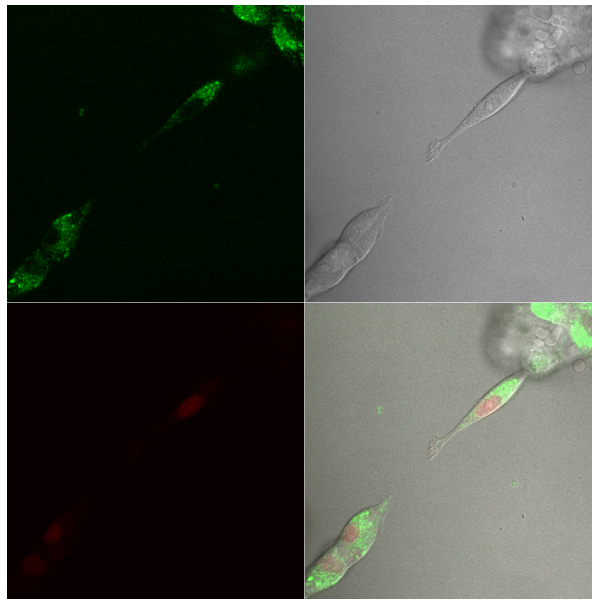


(a)

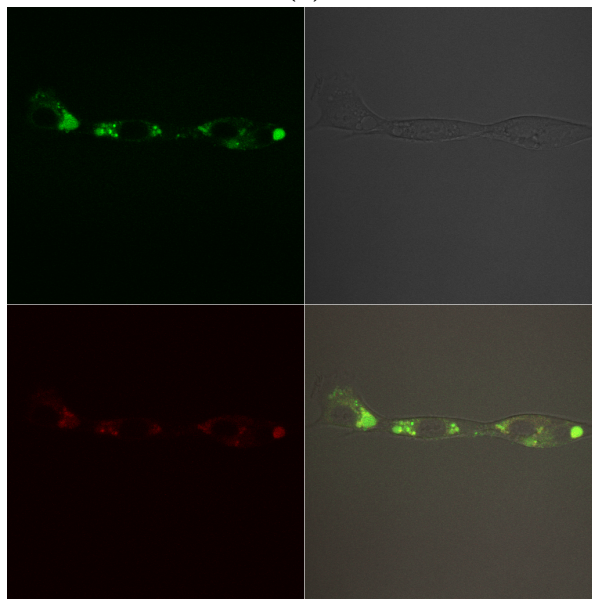


(b)

Figure 4.12: Confocal images of F98 glioma cells after incubation of Ant-OAc with DRAQ5/Lysotracker Red. Ant-OAc is represented in green, and the stains in red. The images documents localization in cytoplasm, but outside the nucleus. Cells marked with DRAQ5 in (a), and cells with Lysotracker Red in (b).

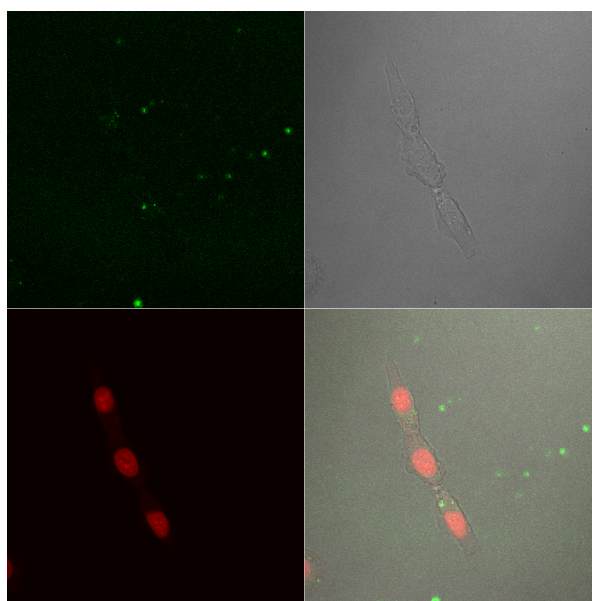


(a)

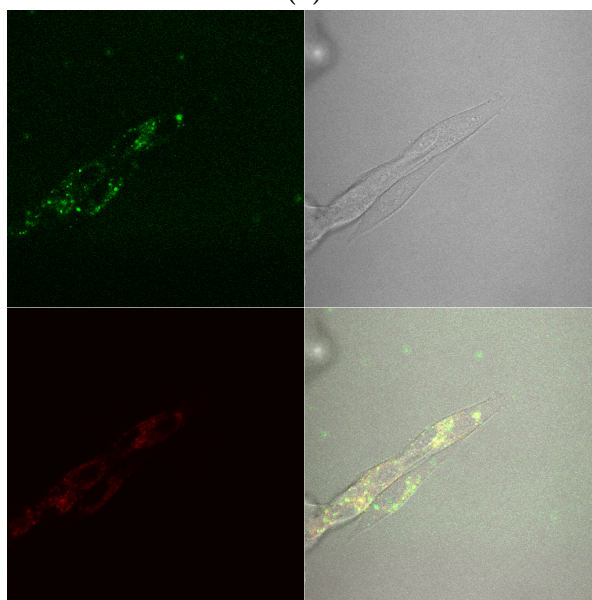


(b)

Figure 4.13: Confocal images of F98 glioma cells after incubation of Ant-PHEA with DRAQ5/Lysotracker Red. Ant-PHEA is represented in green, and the stains in red. The images documents localization in cytoplasm, but outside the nucleus. Cells marked with DRAQ5 in (a), and cells with Lysotracker Red in (b).



(a)



(b)

Figure 4.14: Confocal images of F98 glioma cells after incubation of DBB₂-OAc with DRAQ5/Lysotracker Red. DBB₂-OAc is represented in green, and the stains in red. The images documents localization in cytoplasm, but outside the nucleus. Cells marked with DRAQ5 in (a), and cells with Lysotracker Red in (b).

4.5 Localization of chromophores in CHO-K1 hamster ovary cells

The localization of DBB₂-OAc, Ant-PHEA and Ant-PIm in CHO-K1 hamster ovary cells were also investigated using a confocal laser scanning microscope (Zess LSM 5 Duo, Zeiss LSM 510 META, Zeiss LSM 5 Live, Germany) (Fig. 3.5). Markers for confocal microscopy were added for detection of cell components. The marker for DNA detection was DRAQ5 (1 μ M, 2 ml, 15 min, 37°C, 5% CO₂), and for lysosomes LysoTracker Red (50 nM, 1 ml, 1 h, 37°C, 5% CO₂).

The analysis was performed with a Plan-Apochromate 63x/1.4 oil DIC objective, live cell images were acquired in growth medium (37°C). One channel was used for the chromophores with an Argon/2 laser (488 nm) or a Diode 405-50 laser (405 nm), and another channel for fluorescence markers (DRAQ5 and LysoTracker Red) with a DPSS 561-10 laser (561 nm).

The confocal images of Ant-PIm (10 μ M, 2 ml, 24 h, 37°C, 5% CO₂) together with DNA- and lysosome staining are presented in Fig. 4.15. Ant-PIm seems to be almost localized inside the nucleus (Fig. 4.15a), along within the lysosomes (Fig. 4.15b). The cells in Fig. 4.15a are ‘rolled up’ and possibly dying, which might be the reason Ant-PIm has ‘leaked’ into the nucleus in these cells. This is also the case for the ‘rolled up’ cell in Fig. 4.15b.

A weak fluorescence signal was acquired for DBB₂-OAc incubation in F98 cells. This chromophore was investigated again, but for the second time incubated in CHO-K1 cells (Fig. 4.16).

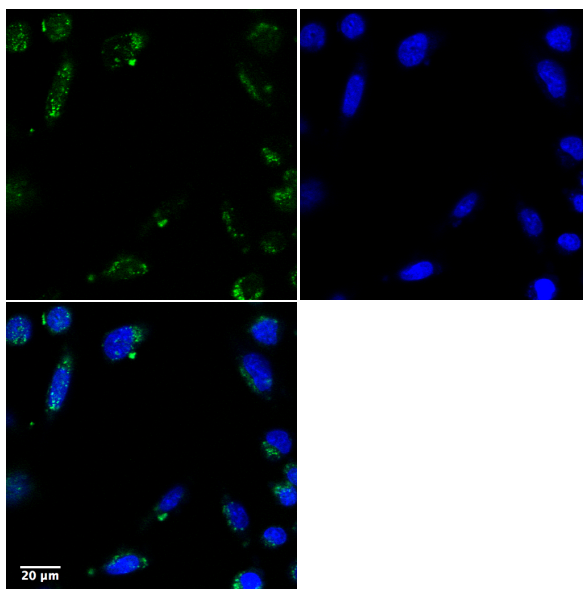
The confocal images of DBB₂-OAc (10 μ M, 2 ml, 24 h, 37°C, 5% CO₂) together with DNA- and lysosome staining are presented in Fig. 4.16. The figures document a not completely dissolved chromophore, and it seems like DBB₂-OAc localizes in some other cellular compartment than LysoTracker Red (e.g. mitochondria or vacuoles).

A stronger concentration of Ant-PHEA was chosen than for Ant-PIm and DBB₂-OAc. This was reasoned after poor results from PDT-experiments using Ant-PHEA (10 μ M) (Section 4.1, Fig. 4.2).

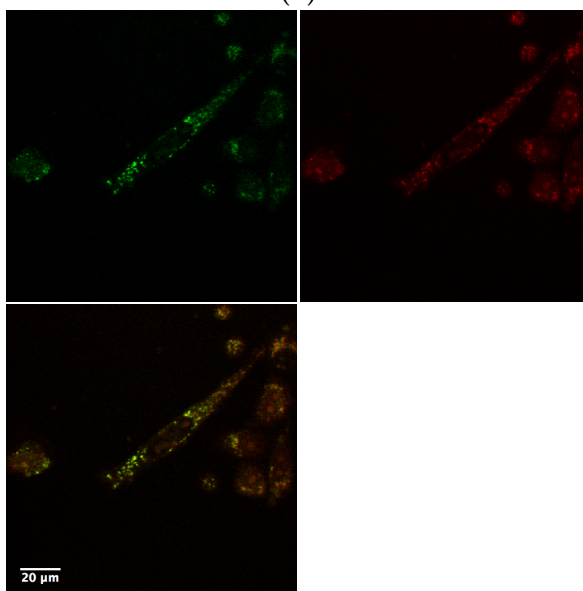
The confocal images of Ant-PHEA (50 μ M, 2 ml, 24 h, 37°C, 5% CO₂)

together with DNA- and lysosome staining are presented in Fig. 4.17. The images documents the localition of Ant-PHEA in cytoplasmic vesicles which seems to correspond to the lysosomes, and not in the nucleus.

Ant-PIIm and Ant-PHEA were localized outside the cell nucleus in living CHO-K1 cells, and seem to be localized somewhat in the lysosomes with Lyso-tracker Red. Figures C.8-C.10 illustrates some colocalization for Ant-PIIm and Ant-PHEA with Lyso-tracker Red, and very little with DRAQ5. Figure C.7 documents colocalization for Ant-PIIm and DRAQ5 in cells that seem to be dying. Corresponding values for colocalization is presented in Tabel 4.1. DBB₂-OAc fluorescences weaker, but seems to be localized in other cellular compartments than Lyso-tracker Red (e.g. mitochondria or vacuoles). This hypothesis is supported by the rather low colocalization values for CHO-K1 cells in Table 4.1 for Lyso-tracker Red (18.15%) and DRAQ5 (3.48%) especially.

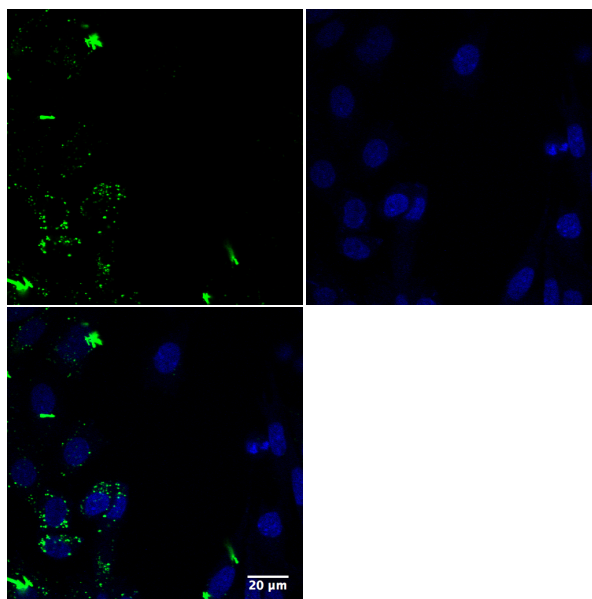


(a)

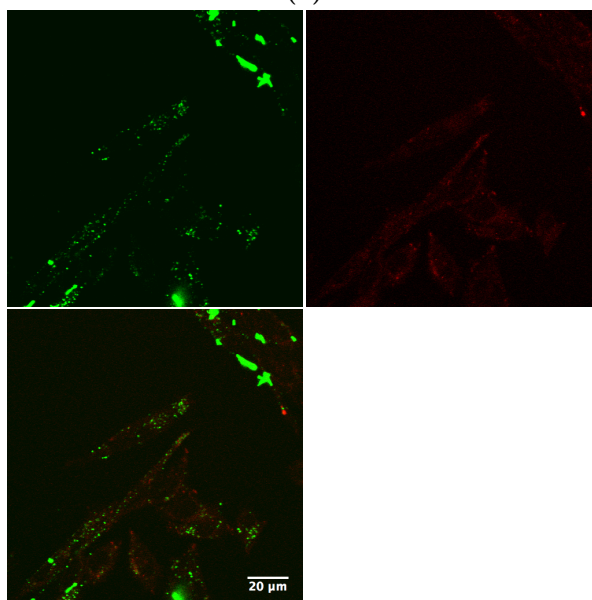


(b)

Figure 4.15: Confocal image of CHO-K1 glioma cells after incubation of Ant-P1m with DRAQ5/Lysotracker Red. Ant-P1m is represented in green, DRAQ5 in blue, and Lysotracker Red in red. The images documents localization in cytoplasm, and somewhat in nucleus in (a). Ant-P1m seems to be localized in lysosomes with Lysotracker Red. Cells marked with DRAQ5 in (a), and cells with Lysotracker Red in (b).



(a)



(b)

Figure 4.16: Confocal image of CHO-K1 glioma cells after incubation with DBB₂-OAc with DRAQ5/Lysotracker Red. DBB₂-OAc is represented in green, DRAQ5 in blue, and Lysotracker Red in red. The images documents localization in cytoplasm, but outside the nucleus. DBB₂-OAc seems to not be localized in the lysosomes with Lysotracker Red, but rather in other cell compartments (for example mitochondria or vacuoles). Cells marked with DRAQ5 in (a), and cells with Lysotracker Red in (b).

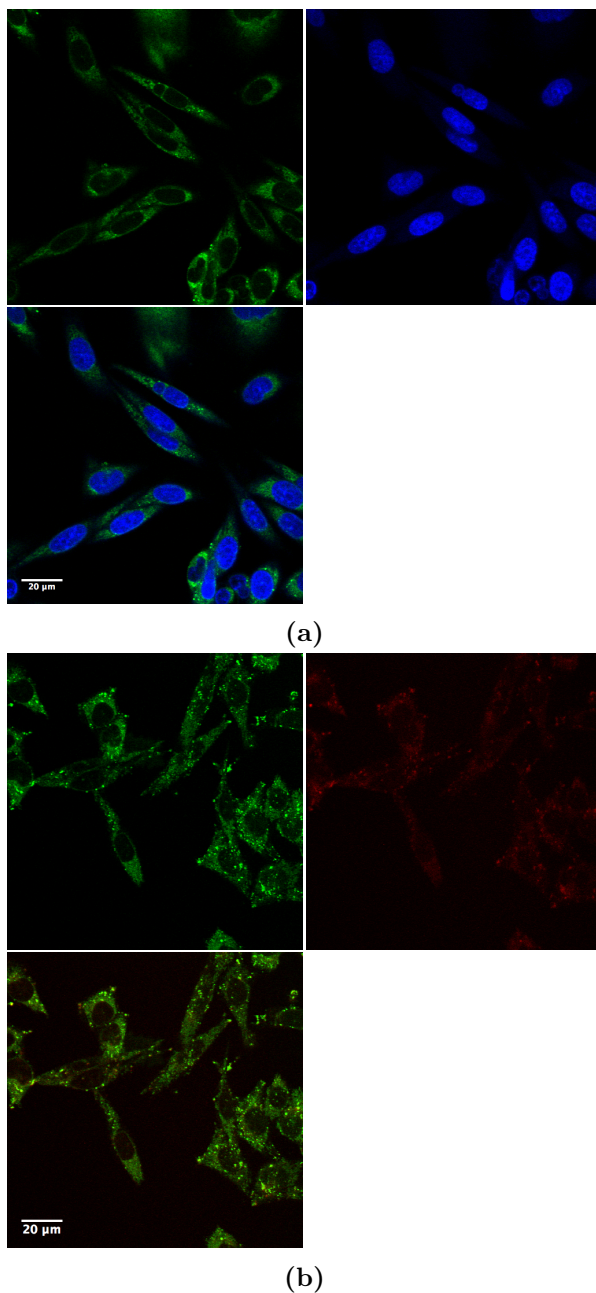


Figure 4.17: Confocal image of CHO-K1 glioma cells after incubation with Ant-PHEA with DRAQ5/Lysotracker Red. Ant-PHEA is represented in green, DRAQ5 in blue, and Lysotracker Red in red. The images document localization in cytoplasm, but outside the nucleus **(b)**, and partly in nucleus **(a)**. Ant-PHEA seems to be localized in lysosomes with Lysotracker Red. Cells marked with DRAQ5 in **(a)**, and cells with Lysotracker Red in **(b)**.

4.6 Colocalization of chromophore and fluorescence stain

The possibility of colocalization of the chromophores with the DNA- and lysosome marker was suggested after obtaining confocal images of Ant-OAc and Ant-PHEA in F98 glioma cells (Section 4.4).

Therefore, colocalization for Ant-OAc, Ant-PHEA, DBB₂-OAc in F98 cells along with DBB₂-OAc, Ant-PIIm and Ant-PHEA in CHO-K1 cells, all tested after adding of DRAQ5 and LysoTracker Red, were investigated (Table 4.1).

The images for each channel (chromophore in channel 2, stain in channel 3) were plotted in gray-scale, and the threshold values were decided by looking at the gray-scale value from the background of each image. The two images for each sample were multiplied to a binary map showing colocalization of chromophore and DRAQ5/LysoTracker Red. Examples from the colocalization results in F98 and CHO-K1 cells are presented in Figs. 4.18 and 4.19 respectively, while all the colocalization images Table 4.1 is based on are presented in Appendix C. These images illustrates the calculations which Table 4.1 is based upon.

All together, the calculated results using the colocalization factor, C_f , defined as the following, are summerized in Table 4.1 (based on the confocal images in Section 4.4 and 4.5).

$$C_f = \frac{N_{cp}}{(N_2 + N_3) - N_{cp}} \cdot 100, \quad (4.2)$$

where N_{cp} is the number of colocalized pixels, N_2 is the number of pixels greater than the threshold value for the channel 2 image, and N_3 is the number of pixels greater than the threshold value for the channel 3 image.

Table 4.1: Results of colocalization calculations. C_f is the colocalization factor. Each calculation is based on one confocal image including chromophore and stain, and these are the same images as presented in Sections 4.4 and 4.5.

Cell line	Chromophore	Stain	C_f (%)
F98	DBB ₂ -OAc	DRAQ5	0.08
		Lysotracker Red	23.39
	Ant-OAc	DRAQ5	4.26
		Lysotracker Red	40.43
	Ant-PHEA	DRAQ5	1.09
		Lysotracker Red	43.13
CHO-K1	DBB ₂ -OAc	DRAQ5	3.48
		Lysotracker Red	18.15
	Ant-PIIm	DRAQ5	40.89
		Lysotracker Red	32.14
	Ant-PHEA	DRAQ5	12.02
		Lysotracker Red	29.74

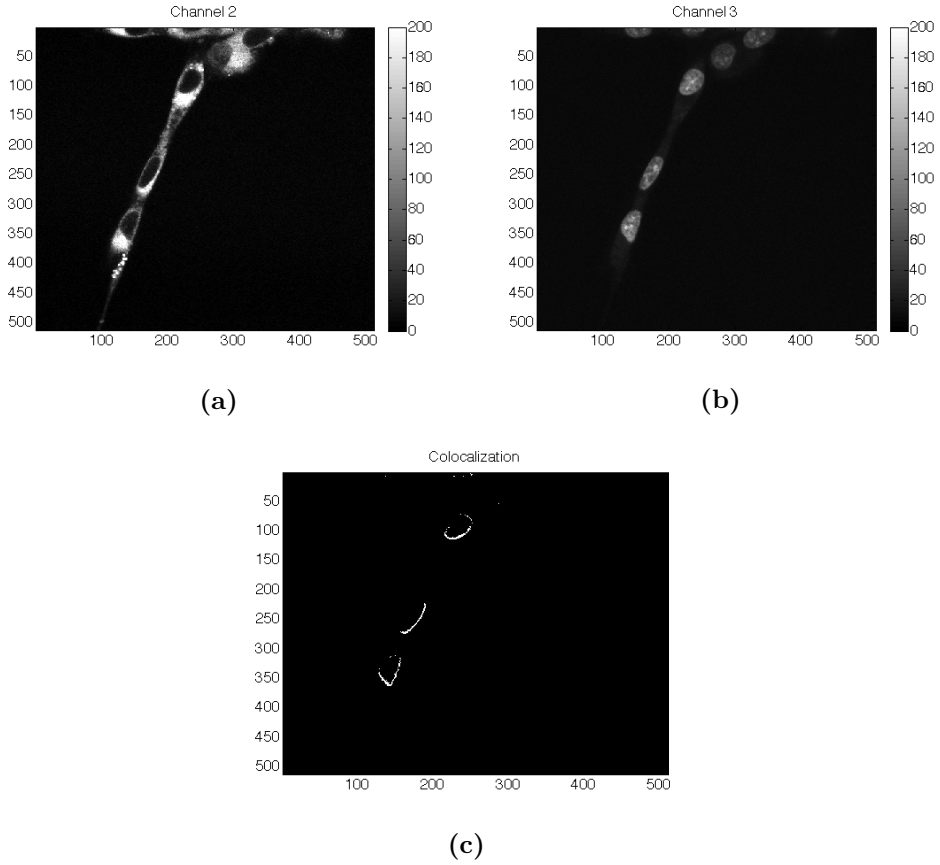


Figure 4.18: Colocalization of Ant-OAc with DRAQ5 in F98 cells based on confocal images in Fig. 4.12a. The gray-scale version of the channel 2 image with Ant-OAc in (a), the gray-scale version of the channel 3 image with DRAQ5 in (b), and the binary map of (a) multiplied with (b) (threshold value of > 60 for both) in (c).

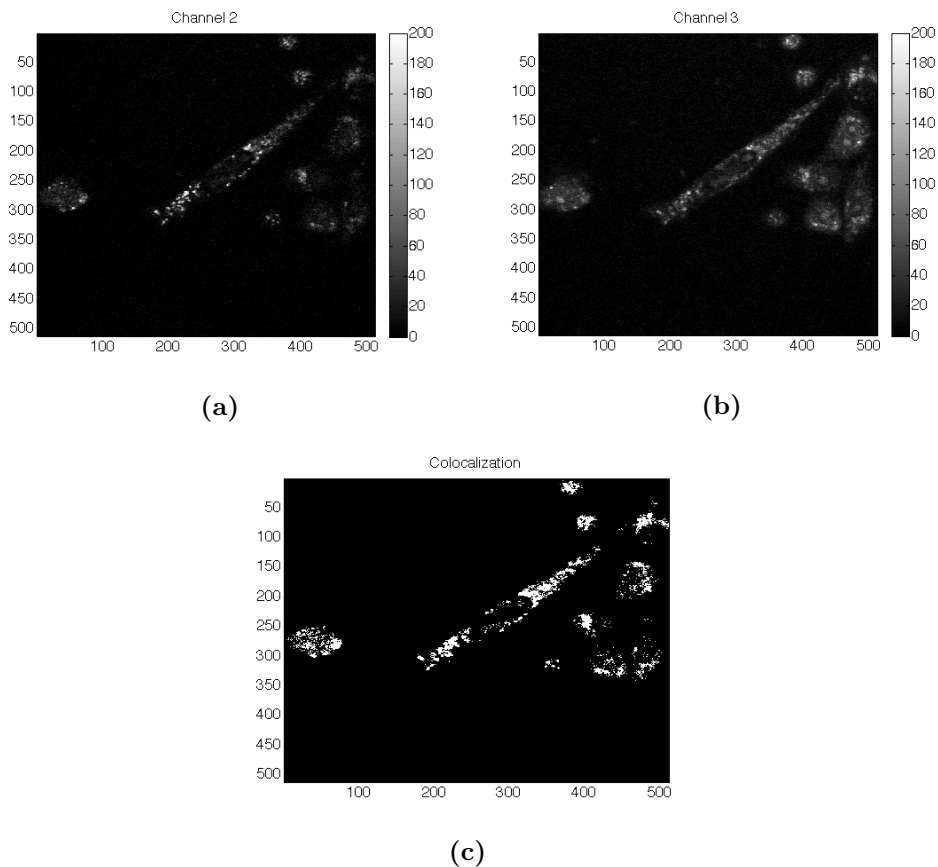


Figure 4.19: Colocalization of Ant-PIm with Lysotracker Red in CHO-K1 cells based on confocal images in Fig. 4.15b. The gray-scale version of the channel 2 image with Ant-PIm in (a), the gray-scale version of the channel 3 image with Lysotracker Red in (b), and the binary map of (a) multiplied with (b) (threshold value of > 30 for both) in (c).

Discussion

5.1 CHO-K1 cell death following PDT with continuous light delivery

5.1.1 Ant-PIIm

The mean lethal dose, LD_{50} , is reached already before 1 min of illumination (435 nm, 12.9 mW/cm²) in Ant-PIIm (10 μ M, 24 h) incubated CHO-K1 cells, as shown in Fig. 4.1. This efficacy is probably partly due to the large dark toxicity (effects of Ant-PIIm alone; 10 μ M) of this PS; $\sim 40\%$ cell death.

The dark toxicity, as already mentioned, results in $38.0 \pm 3.5\%$ cell death, and is relatively high compared to hexyl 5-aminolevulinate acid (HAL)-incubated cancer cells recently described by Helander *et al.* (2014). The HAL dark toxicity in these five tested human cell lines (A431, A549, HeLa S3, T24, WiDr) varies between 10 – 25%. [53] However, the present Ant-PIIm data harmonize with the dark toxicity of DBB₂-OAc $\sim 60\%$ incubated (10 μ M, 24 h) rat glioma cells (F98) observed in unpublished results by Odrun Gederass *et al.* (Appendix D, Fig. D.1).

5.1.2 Ant-PHEA

The Ant-PHEA chromophore has an evident less dark toxicity effect compared to Ant-PIm with as little as 10% cell death for drug-only treated cells, as presented in Fig. 4.2. However, this chromophore also seems to be less effective as a PS compared to Ant-PIm for light treatments longer than 2 – 3 minutes.

The overall light dose required to kill close to 90% (30 min of light) of CHO-K1 cells without any chromophores, will be discussed later.

For the 10 μM and 50 μM Ant-PHEA incubated cells an evident decrease was observed after both 1, 2 and 3 min of light, and can be explained by the DNA-repairing system which starts immediately effecting the cell survival. Similar effects were also observed in human colon carcinoma cells (WiDr) by Odrun Gederaas *et al.* (2000), [54] and in unpublished results by Linda Helander (NTNU).

The increase of cell survival of about 60% alive after 30 min of light (Fig. 4.2) may be explained by the DNA-repairing system in cells which seems to work well until 5 min of light, and shows stable conditions until 30 min of light.

However, after higher Ant-PHEA concentration (100 μM) in combination with e.g. a light dose of 30 min, the cell damage is too high for the DNA-repairing systems, resulting in a cell survival of only $\sim 10\%$.

The dark toxicity was not measured for 50 μM and 100 μM Ant-PHEA incubated cells. This should be done in later experiments.

5.1.3 CHO-K1 sensitivity to blue light

Some unexpected and strange results have been achieved for light-only treated CHO-K1 cells (435 nm, 12.9 mW/cm²). In experiments performed in January 2015 and two in April 2015, light-only treated cells have shown survival curves similar to cells undergoing PDT (Fig. 5.1).

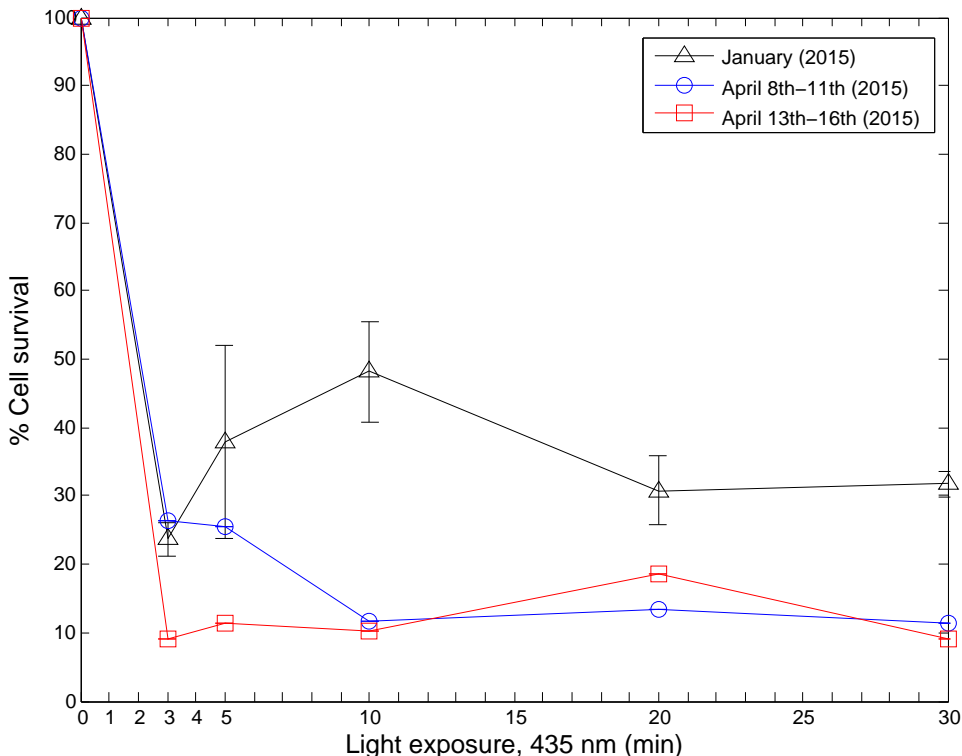


Figure 5.1: Cell survival curve for CHO-K1 cell line after light-only treatment (January in duplicates, both from April in singles).

These results might be due to this cell line being very sensitive to light alone. The publication by Stamato and Waldren (1977) looking at UV-sensitivity of CHO-K1 and variations of that cell line. They stated that CHO-K1 cells deattach from the bottom of dishes if radiated with UV-light. [55] The lamp used in the master thesis work emits strongly at a wavelength of 435 nm which is close to the UV-range (10 – 400 nm) (emission spectrum of LumiSource lamp in Appendix G). The publication by Stamato and Waldren from 1977 never states the exact wavelength they used, but it might be possible that the same effects can be caused by illumination at 435 nm, especially if the dose of radiation is significant higher.

The LD_{50} dose for UV-irradiated CHO-K1 cells was measured to be 45 ergs/mm². With 1 erg= 100 nJ, making this equivalent to 0.45 mWs/cm². The

LumiSource lamp for 1 min gives a dose of: $12.9 \text{ mW/cm}^2 \cdot 60 \text{ s} = 774 \text{ mWs/cm}^2$, which is a great deal more than D_{50} . It is possible that the cells deattached during illumination, and was removed with PBS-washing afterwards. Of that reason it might be few cells which were ready for MTT assay the next day. The cells were studied in a regular light microscope the day after illumination, and before MTT assay. It was noticed very few cells in dishes with light-only treatment, and the cells looked good and alive. This observation was important and strengthen my hypothesis.

Cells incubated with Ant-PHEA (10 μM , 50 μM , 100 μM) and illuminated with blue light (5 – 30 min) do not result in same amounts of cell death, except for 100 μM at 30 min (Fig. 4.2). Thus indicating little effect of the cell-deattachement described above. One reason might be because the chromophore absorbs photons from radiation, and not what it is that causes deattachment.

The curve for cells only treated with light in Fig. 4.1 is based on an independent experiment conducted with only these samples, which is not standard procedure. This curve is not representative since it was not a part the experiments where Ant-PIIm or Ant-PHEA were included.

5.2 DNA damage following Ant-PIm and Ant-PHEA induced PDT

The comet assay was performed to investigate DNA damage caused upon CHO-K1 cells following Ant-PIm and Ant-PHEA induced PDT. It scores single-strand breaks (SSB) and alkali-labile sites (ALS) in living cells posttreatment, and is generally believed that DNA migration (visible as comet tails' in the microscope) in electric field, is proportional to SSBs, and an estimation of DNA-toxicity. [56]

No significant difference among the control (untreated cells), light-only, drug-only, and PDT samples were found in the comet assay (Fig. 4.3). This indicates no DNA damage caused by light, drug, or light-drug combinations. Similar results were achieved by McNair *et al.* (1997) for the photosensitizers HpD (hemaporphyrin derivative), and mTHPC (*meso*-tetrahydroxyphenylchlorin). [57]

Epe *et al.* (1993) established how a range of different photosensitizers expressed DNA damage similar to that caused by singlet oxygen in cell-free systems. These results support the general belief that cell death following PDT is mainly caused by singlet oxygen formation. [58] However, singlet oxygen has proven to have a short lifetime and diffusion distance in cells ($\leq 0.6 \mu\text{s}$, $\leq 0.07 \mu\text{m}$). The part of the cell damaged by creation of singlet oxygen is hence highly dependent on localization of the drug inside the cell. [59] Thus, it is unlikely for singlet oxygen generated outside the nucleus to reach the DNA without reacting with something else, or becoming quenched first.

According to the present study, both Ant-PIm and Ant-PHEA have been established to localize outside the nucleus in cytoplasmic vesicles, as discussed in Section 5.4. The lack of detected DNA damage by the comet assay (Fig. 4.3) documents the confocal microscopy results for both chromophores. This suggest a little possibility for Ant-PIm and Ant-PHEA leading to mutations, for even though SSBs and ALSs are considered to be rapidly repaired and unlikely to lead to cell death, is there a slight chance they might be repaired incorrectly and lead to mutation. [60]

5.3 Spectroscopic measurements of DBB₂-OAc, Ant-PIm and Ant-PHEA

5.3.1 Absorbance

The absorption spectra of Ant-PIm and Ant-PHEA seem to be almost identical, while the one for DBB₂-OAc differ from the two others (Fig. 4.4). The shape of the absorption spectra of Ant-PHEA is consistent with same absorption spectra for identical chromophore in H₂O published by Cyrille Monnereau *et al.* (2012). [26]

The molecules' structural formula for Ant-PIm and Ant-PHEA includes the same backbone and very similar oligomeric arms (Table 2.1), only the end-group of the arms are different. This may explain the similar absorption curves.

The DBB₂-OAc chromophore is blue shifted compared to the two Ant-compounds. The shift in absorption spectrum might be due to its diyne bridge connecting two dibromobenzene moieties.

5.3.2 Excited state absorbance

The excited state absorption signal for DBB₂-OAc is clearly stronger than for the two anthracene compounds Ant-PIm and Ant-PHEA (Fig. 4.8a). This is partly due to the DBB₂-OAc solution having a higher concentration. Another reason might be the solvent for DBB₂-OAc (a mixture of dH₂O and THF), while the two others were dissolved in dH₂O.

The triplet state is crucial for PDT-mechanisms to take place (formation of singlet oxygen and other ROS) (Section 2.4). Hence, the good signal achieved for DBB₂-OAc suggest the compound as a good candidate for PDT (Fig. 4.5). This is consistent with previously conducted PDT-experiments for this chromophore on F98 cells (Appendix D).

The poor signals for Ant-PIm and Ant-PHEA (Figs. 4.6 and 4.7) might suggest that they are not good candidates for PDT (tested on F98 and CHO-K1 cells) based on the low yield of intersystem crossing and their short lived triplet state. [61] The signal for Ant-PIm is similar in shape to the signal for Ant-PHEA, but also stronger (Fig. 4.8b). The concentration of Ant-PHEA

solution used in this experiment was lower than the one for Ant-PIm, which is also why the signal is weaker for Ant-PIm. The excited state absorption spectra of Ant-PIm and Ant-PHEA should be recorded with a concentration of 50 μM for both in a mixture of dH_2O and THF to be able to fully compare it with the spectrum of DBB₂-OAc. The anthracene compounds were not initially made to work as photosensitizers, but rather as dyes for fluorescence imaging. [26]

5.3.3 Transient state lifetime

The transient state lifetime was only detected for DBB₂-OAc since a strong and long lived ESA signal is needed to allow such characterization.

A suitable photosensitizer should have a long triplet lifetime. [62] DBB₂-OAc was found to have a triplet lifetime in order of 10^{-4} s, which is not particularly long, but within the general range of 10^{-6} s to 1 s. [31, 34]

5.3.4 Singlet oxygen lifetime

Singlet oxygen, $^1\text{O}_2$, is generally accepted to be an important ROS in the cell death process caused by PDT *in vitro*. [62]

In the present study the chromophore solutions were without air as a reference to samples with air which is the one of interest. The singlet oxygen lifetime was recorded for DBB₂-OAc (50 μM , 64 averages) and Ant-PIm (25 μM , 128 averages) (Figs. 4.10 and 4.11). It was decided to not repeat the singlet oxygen lifetime measurement for Ant-PHEA, since it gave similar ESA results as for Ant-PIm, and thereby suggesting similar results for singlet oxygen lifetime.

The $^1\text{O}_2$ signal is weak with a lot of noise for Ant-PIm (Fig. 4.11). The singlet oxygen detected for samples with air are higher compared to signals from samples without air (more signal > 0 compared to signal < 0), although this difference is almost negligible. The results suggests another cell death mechanism after incubating with Ant-PIm (Section 4.1) compared to mechanism as from singlet oxygen. The death might be caused by a type I reaction (death by ROS other than $^1\text{O}_2^*$), instead of type II (death by $^1\text{O}_2^*$). [14]

The signal for DBB₂-OAc is more evident (Fig. 4.10), and it is to be believed that more singlet oxygen is created from the reaction between DBB₂-OAc and

light, compared to Ant-PIm and light. Mark Jarvi *et al.* (2012) documented a clear connection between the generation of $^1\text{O}_2$ and cell death after PDT. His group presented negligible cell death in absence of singlet oxygen. [63]

The difference in concentration of the two chromophores might affect the results, but it is reasonable to believe that even with same concentration DBB₂-OAc would show more evident signals than Ant-PIm. This assumption is based on the large difference in ESA signals as illustrated in Fig. 4.8a.

It is reason to assume that cell death by DBB₂-OAc induced PDT is caused by generation of $^1\text{O}_2$, while Ant-PIm induced PDT leads to cell death caused by other reactive oxygen species, and further explain the negligible singlet oxygen luminescence signals for Ant-PIm.

5.4 Localization of chromophores in F98 and CHO-K1 cells

The cellular localization of Ant-OAc has been investigated using F98 rat glioma cells, while the localization of Ant-PIm has been investigated using CHO-K1 hamster ovary cells. The cellular localization of DBB₂-OAc and Ant-PHEA were investigated using both cell lines.

Ant-OAc was localized outside the cell nuclues in F98, and seem to be localized in the lysosomes detected by Lysotracker Red. A relative high colocalization factor (40.43%) was found for Ant-OAc with Lysotracker Red (Table 4.1) compared to the colocalization with DRAQ5 (4.26%).

Ant-PIm seems to be partly localized inside the nuclues (Fig. 4.15a), along within the lysosomes (Fig. 4.15b) in CHO-K1. The cells in Fig. 4.15a are ‘rolled up’ and possibly dying, which might be the reason Ant-PIm has ‘leaked’ into the nuclues in these cells. This is also the case for the ‘rolled up’ cell in Fig. 4.15b. While the living, stretched out cell in Fig. 4.15b seems to not have Ant-PIm in the nucleus, but in the lysosomes with Lysotracker Red. This is supported by the values calculated for C_f (Table 4.1) for Ant-PIm, and from Figs. C.7 and C.8. The C_f values for Ant-PIm suggests that the chromophore mostly localize inside the nucleus of the cells, however, these results may be misleading. Figure 4.15b is the most representative image of Ant-PIm,

since this one is of a living cell and C_f is relative high for colocalization with LysoTracker Red. Therefore, Ant-PIm localize in some cellular compartment in the cytoplasm, most likely lysosomes, but might also penetrate the nuclear “envelope” after some time and/or when the cells are dying.

It seems that CHO-K1 and F98 cells easily take up Ant-PHEA, however not into the nucleus (Fig.4.17), but rather into cytoplasmic vesicles, such as within lysosomes (LysoTracker Red) which is supported by the high values of colocalization with LysoTracker Red presented in Table 4.1 (29.74% and 43.13%).

It is difficult to document where DBB₂-OAc is localized in the cancer cells due to its weak fluorescence, but it seems to be localized in the lysosomes (LysoTracker Red) in F98 cells (Fig. 4.14), while in other cell compartments (e.g. mitochondria or vacuoles) in CHO-K1 cells (Fig. 4.16). This chromophore fluoresces weakly which is evident for the C_f values in Table 4.1, still it shows a clearly higher colocalization with LysoTracker Red compared to DRAQ5 (Table 4.1).

5.5 Chromophores as a potential photosensitizer

A summarization of the chromophores and their properties is given in Table 5.1.

DBB₂-OAc is the best candidate for PDT as it has proven to lead to cell death (Appendix D) after illumination of blue light, it has a relative long lived triplet state, and generates singlet oxygen when excited. A drawback might be that it is hard to localize when using fluorescence microscopy, and its dark toxicity is 41% (Appendix D) which is too high for an ideal PS.

Ant-PIm might also be a good candidate for PDT if its dark toxicity is improved. It seems to be able to kill cells by another process than singlet oxygen, and it has the advantage of fluorescing strongly.

Table 5.1: A summarization of the chromophores and their properties. ‘Dark toxicity’ is found for a concentration of 10 μM for all three chromophores (DBB₂-OAc, Ant-PIIm, Ant-PHEA). The excited state absorption (ESA) is characterize as *good/weak* signal.

Chromophore (10 μM)	Localization	ESA	$^1\text{O}_2^*$ lifetime	Dark toxicity ($\pm\text{SD}$)
DBB ₂ -OAc	cytoplasm/lysosomes	good	~ 1 s	41%
Ant-PIIm	cytoplasm/lysosomes	weak	~ 0 s	$38.0 \pm 3.5\%$
Ant-PHEA	cytoplasm/lysosomes	weak	-	$12.9 \pm 6.6\%$
Ant-OAc	cytoplasm/lysosomes	-	-	-

5.6 Future work

- The single-hit multi-target model should be taken under consideration after more PDT-experiments have been conducted. Hit-theory is important for this kind of experiments, but this early on it was found to not be relevant.
- The oligomeric chromophore DBB₂-PHEA, which have the same backbone as DBB₂-OAc and substituents as Ant-PHEA, should be further tested in PDT-survival experiments in the future. Its triplet ESA signal and measurements of singlet oxygen lifetime is also of great interest. There are several reasons to believe this chromophore will be an efficient PS.
- Some modifications on Ant-PIIm, if possible, should be performed to decrease the dark toxicity of the molecule, and possibly make it as a candidate for PDT.

Conclusions

- Ant-PHEA seems to be better suited as a dye for fluorescence imaging than as a photosensitizer. The chromophore fluoresced particularly strong during confocal microscopy.
- Ant-PIIm showed promising properties as a photosensitizer. Its anthracene core makes it also suitable for fluorescence imaging. However, its dark toxicity must be severely reduced for it to be a good candidate for both PDT and fluorescence imaging.
- Spectroscopic data acquired for DBB₂-OAc suggest that this chromophore is suitable for photodynamic therapy and able to produce singlet oxygen from its triplet state. This coincides with pilot studies performed on this chromophore (Appendix D). However, a reduction of its dark toxicity is necessary for it to be a good candidate for PDT.
- All four chromophores investigated in the thesis work are able to localize inside F98 and CHO-K1 cells. They are all localized in some cellular compartment in the cytoplasm. However, Ant-PIIm also seems to be able to penetrate the nuclear “envelope” after some time (24 h) and/or when the cell is dying.

Bibliography

- [1] O. Raab. Ueber die wirkung fluorescirender stoffe auf infusorien. *Z. Biol.*, 39:524–546, 1900.
- [2] T. J. Dougherty. Photodynamic therapy (pdt) of malignant tumors. *Critical reviews in oncology/hematology*, 2(2):83–116, 1984.
- [3] H. Jesionek and H. von Tappeiner. Zur behandlung der hautcarcinome mit fluoreszierenden stoffen. *Dtsch. Arch. Klin. Med.*, 82:223–226, 1905.
- [4] H. Höningsmann. History of phototherapy in dermatology. *Photochem. Photobiol. Sci.*, 12, 2013.
- [5] G. Bock and S. Harnett. *Photosensitizing compounds: their chemistry, biology, and clinical use*. John Wiley Sons, 1989.
- [6] J. F. Kelly, M. E. Snell, and M. C. Berenbaum. Photodynamic destruction of human bladder carcinoma. *Br. J. Cancer*, 31:237–244, 1975.
- [7] D. S. Rassmussen-Taxdak, G. E. Ward, and F. H. J. Figge. Fluorescence of human lymphatic and cancer tissues following high doses of intravenous hematoporphyrin. *Cancer*, 8:78–81, 1955.
- [8] R. L. Lipson and E. J. Baldes. The photodynamic properties of a particular hematoporphyrin derivative. *Arch. Dermatol.*, 82:508–516, 1960.

- [9] I. Diamond, S. G. Granelli, A. F. McDonagh, S. Nielsen, C. B. Wilson, and Jaenicke R. Photodynamic therapy of malignant tumours. *The Lancet*, 300:1175–1177, 1972.
- [10] T. J. Dougherty, G. B. Grindey, R. Fiel, K. R. Weishaupt, and D. G. Boyle. Photoradiation therapy. ii. cure of animal tumors with hematoporphyrin and light. *J. Natl. Cancer Inst.*, 55, 1975.
- [11] J. F. Kelly and M. E. Snell. Hematoporphyrin derivative: a possible aid in the diagnosis and therapy of carcinoma of the bladder. *J. Urol.*, 115:150–151, 1976.
- [12] D. E. J. G. J. Dolmans, D. Fukumura, and R. K. Jain. Photodynamic therapy for cancer. *Nature Reviews Cancer*, 3:380–387, 2003.
- [13] T. J. Dougherty, J. E. Kaufman, A. Goldfarb, K. R. Weishaupt, D. Boyle, and A. Mittelman. Photoradiation therapy for the treatment of malignant tumors. *Cancer Research*, 38:2628–2635, 1978.
- [14] P. N. Prasad. *Introduction to Biophotonics*. John Wiley & Sons, 2003.
- [15] N. Ramakrishnan, M. E. Clay, L. R. Friedman, A. R. Antunez, and N. L. Oleinick. Post-treatment interactions of photodynamic and radiation-induced cytotoxic lesions. *Photochem. Photobiol.*, 52(3):555–559, 1990.
- [16] J. D. Miller, E. D. Baron, H. Scull, A. Hsia, J. C. Berlin, T. McCormick, V. Colussi, M. E. Kenney, K. D. Cooper, and N. L. Oleinick. Photodynamic therapy with the phthalocyanine photosensitizer pc 4: The case experience with preclinical mechanistic and early clinical-translational studies. *Toxicology and Applied Pharmacology*, 224:290–299, 2007.
- [17] E. J. Hall and A. J. Giaccia. *Radiobiology for the Radiologist*. Wolters Kluwer, Lippincott Williams & Wilkins, 2012.
- [18] S. R. Bolsover, J. S. Hyams, E. A. Shephard, H. A. White, and C. G. Wiedemann. *Cell Biology: A short course*. John Wiley & Sons, 2004.

- [19] Rolf F. Barth. Rat brain tumor models in experimental neuro-oncology: the 9l, c6, t9, f98, rg2 (d74), rt-2 and cns-1 gliomas. *Journal of Neuro-Oncology*, 36:91–102, 1998.
- [20] D. B. Paul, R. F. Barth, W. Yang, G.-H. Shen, J. Kim, and P. L. Triozzi. B7.1 expression by the weakly immunogenic f98 rat glioma does not enhance immunogenicity. *Gene Therapy*, 7:993–999, 2000.
- [21] N. E. Lewis, X. Liu, Y. Li, H. Nagarajan, G. Yerganian, E. O’Brien, A. Bordbar, A. M. Roth, J. Rosenbloom, C. Bian, M. Xie, W. Chen, N. Li, D. Baycin-Hizal, H. Latif, J. Forster, M. J. Betenbaugh, I. Famili, X. Xu, J. Wang, and B. O. Palsson. Genomic landscapes of chinese hamster ovary cell lines as revealed by the cricetus griseus draft genome. *Nature Biotechnology*, 31(8):759–765, 2013.
- [22] T. T. Puck, S. J. Cieciora, and A. Robinson. Genetics of somatic mammalian cells. iii. long-term cultivation of euploid cells from human and animal subjects. *The Journal of Experimental Medicine*, 108, 1958.
- [23] Percell Biolytica AB. *Growth of Recombinant and Non-recombinant CHO-cells*.
- [24] ATCC. F98 egfr (atcc crl-2948). <http://www.lgcstandards-atcc.org/products/all/CRL-2948.aspx>. Accessed: 2015-03-20.
- [25] ATCC. Cho-k1 (atcc ccl-61). <http://www.lgcstandards-atcc.org/products/all/CCL-61.aspx>. Accessed: 2015-03-20.
- [26] C. Monnereau, S. Marotte, P.-H. Lanoë, O. Maury, P. L. Baldeck, D. Kreher, A. Favier, M.-T. Charreyre, J. Marvel, Y. Leverrier, and Andraud C. Water-soluble chromophores with star-shaped oligomeric arms: synthesis, spectroscopic studies and first results in bio-imaging and cell death induction. *New J. Chem.*, 36:2328–2333, 2012.
- [27] H. Kaur. *Spectroscopy*. Pragati Prakashan, 2009.
- [28] P. W. Atkins. *The Elements of Physical Chemistry*. Oxford University Press, 1996.

- [29] J. García Solé, L. E. Bausá, and D. Jaque. *An Introduction to the Optical Spectroscopy of Inorganic Solids*. John Wiley & Sons, 2005.
- [30] H. H. Jaffe and Albert L. Miller. The fates of electronic excitation energy. *Journal of Chemical Education*, 43(9):469, 1966.
- [31] Joseph R. Lakowicz. *Principles of Fluorescence Spectroscopy*. Springer US, 2006.
- [32] P. Atkins and J. de Paula. *Physical Chemistry for the Life Sciences*. W. H. Freeman and Company, Oxford UK, 2006.
- [33] Wikipedia. Franck-condon-prinzip. <http://de.wikipedia.org/wiki/Franck-Condon-Prinzip>. Accessed: 2015-03-10.
- [34] I. Carmichael and G. L. Hug. Triplet–triplet absorption spectra of organic molecules in condensed phases. *Journal of Physical and Chemical Reference Data*, 15(1):1–250, 1986.
- [35] M. Kasha. Characterization of electronic transitions in complex molecules. *Discuss. Faraday Soc.*, 9:14–19, 1950.
- [36] P. Bilski, M. E. Daub, and C. F. Chignell. Direct detection of singlet oxygen via its phosphorescence from cellular and fungal cultures. In C. K. Sen and L. Packer, editors, *Methods in Enzymology, Volume 352: Redox Cell Biology and Genetics, Part A*. Academic Press, 2002.
- [37] M. Chessin, R. Livingston, and T. G. Truscott. Direct evidence for the sensitized formation of a metastable state of [small beta]-carotene. *Trans. Faraday Soc.*, 62:1519–1524, 1966.
- [38] M. G. Vivas, L. de Boni, L. Gaffo, and C. R. Mendonca. Investigation of ground and excited state photophysical properties of gadolinium phthalocyanine. *Dyes and Pigments*, 101(0):338 – 343, 2014.
- [39] Pawel Mroz, Anastasia Yaroslavsky, Gitika B. Kharkwal, and Michael R. Hamblin. Cell death pathways in photodynamic therapy of cancer. *Cancers*, 3:2516–2539, 2011.

- [40] J. Moan and K. Berg. The photodegradation of porphyrins in cells can be used to estimate the lifetime of singlet oxygen. *Photochemistry and photobiology*, 53(4):549–553, 1991.
- [41] M. Ochsner. Photophysical and photobiological processes in the photodynamic therapy of tumours. *Journal of Photochemistry and Photobiology B: Biology*, 39:1–18, 1997.
- [42] K.-K. Iu and P. R. Ogilby. A time-resolved study of singlet molecular oxygen ($^1\Delta_g$) formation in a solution-phase photosensitized reaction: a new experimental technique to examine the dynamics of quenching by oxygen. *Journal of Physical Chemistry*, 91(6):1611–1617, 1987.
- [43] R. R. Tice, E. Agurell, D. Anderson, B Burlinson, A. Hartmann, H. Kobayashi, Y. Miyamae, E. Rojas, J.-C. Ryu, and Y. F. Sasaki. Single cell gel/comet assay: Guidelines for in vitro and in vivo genetic toxicology testing. *Environmental and Molecular Mutagenesis*, 35:206–221, 2000.
- [44] D. B. Murphy and M. W. Davidson. *Fundamentals of Light Microscopy and Electronic Imaging*. John Wiley Sons, 2013.
- [45] Olympus Corporation. Introduction to confocal microscopy. <http://www.olympusfluoview.com/theory/confocalintro.html>. Accessed: 2015-03-05.
- [46] J. B. Pawley, editor. *Handbook of Biological Confocal Microscopy*. Springer US, 2006.
- [47] Olympus Corporation. Fluorophores for confocal microscopy. <http://www.olympusconfocal.com/theory/fluorophoresintro.html>. Accessed: 2015-05-09.
- [48] P. J. Smith and R. J. Errington. Live cell dna labeling and multiphoton/confocal microscopy. In J. E. Celis, editor, *Cell Biology, Four-Volume Set: A Laboratory Handbook*. Elsevier Academic Press, London, UK, 2006.
- [49] Thermo Fisher Scientific Inc. Lysotracker red dnd-99 - special packaging. <https://www.lifetechnologies.com/order/catalog/product/L7528>. Accessed: 2015-05-09.

- [50] J. Carmichael, W. G. DeGraff, A. F. Gazdar, J. D. Minna, and J. B. Mitchell. Evaluation of a tetrazolium-based semiautomated colorimetric assay: Assessment of chemosensitivity testing. *Cancer Research*, 47:936–942, 1987.
- [51] Johan van Meerloo, Gertjan J.L. Kaspers, and Jacqueline Cloos. Cell sensitivity assays: The mtt assay. In Ian A. Cree, editor, *Cancer Cell Culture*, volume 731 of *Methods in Molecular Biology*, pages 237–245. Humana Press, 2011.
- [52] Tim Mosmann. Rapid colorimetric assay for cellular growth and survival: Application to proliferation and cytotoxicity assays. *Journal of Immunological Methods*, 65:55–63, 1983.
- [53] L. Helander, H. E. Krokan, A. Johnsson, O. A. Gederaas, and K. Plaetzer. Red versus blue light illumination in hexyl 5-aminolevulinate photodynamic therapy: the influence of light color and irradiance on the treatment outcome *in vitro*. *Journal of Biomedical Optics*, 19, 2014.
- [54] O. A. Gederaas, J. W. M. Lagerberg, O.-L. Brekke, K. Berg, and T. M. A. R. Dubbelman. 5-aminolevulinic acid induced lipid peroxidation after light exposure on human colon carcinoma cells and effect of α -tocopherol treatment. *Cancer Letters*, 159, 2000.
- [55] T. D. Stamato and C. A. Waldren. Isolation of uv-sensitive variants of cho-k1 by nylon replica plating. *Somatic Cell Genetics*, 3:431–440, 1977.
- [56] P. Duez, G. Dehon, A. Kumps, and J. Dubois. Statistics of the comet assay: a key to discriminate between genotoxic effects. *Mutagenesis*, 18:159–166, 2003.
- [57] F. I. McNair, B. Marples, C. M. L. West, and J. V. Moore. A comet assay of dna damage and repair in k562 cells after photodynamic therapy using haematoporphyrin derivative, methylene blue, and meso-tetrahydroxyphenylchlorin. *British Journal of Cancer*, 75:1721–1729, 1997.

- [58] B. Epe, M. Pflaum, and S. Boiteux. Dna damage induced by photosensitizers in cellular and cell-free systems. *Mutation Research*, 299:135–145, 1993.
- [59] J. Moan. On the diffusion length of singlet oxygen in cells and tissues. *Journal of Photochemistry and Photobiology, B: Biology*, 6:343–344, 1990.
- [60] J. F. Ward. Dna damage and repair. *Basic Life Sci.*, 58:403–415, 1991.
- [61] J. Zhao, W. Wu, J. Sun, and S. Guo. Triplet photosensitizers: from molecular design to applications. *Chem. Soc. Rev.*, 42:5323–5351, 2013.
- [62] Z. Katona, A. Grofcsik, P. Baranyai, I. Bitter, G. Grabner, M. Kubinyi, and T. Vidóczy. Triplet state spectroscopic studies on some 5,10,15,20-tetrakis(methoxyphenyl)porphyrins. *Journal of Molecular Structure*, 450:41–45, 1998.
- [63] M. T. Jarvi, M. S. Patterson, and B. C. Wilson. Insights into photodynamic therapy dosimetry: Simultaneous singlet oxygen luminescence and photosensitizer photobleaching measurements. *Biophys. J.*, 102:661–671, 2012.
- [64] Rogo-Sampaic. Counting chamber burker. <http://www.rogosampaic.com/Counting-chamber-Burker>. Accessed: 2015-05-12.
- [65] NTNU, Trondheim, Norway. *Labøving nr. 2: Celledyrkning*, 2015.

Appendices

Appendix **A**

Recipes of media

A.1 Growth medium - F98 rat glioma cell line

Dulbecco's Modified Eagles Medium	500 ml
L-glutamine	1.7 ml
Tefal Bovine Serum	50 ml
Peericillin/Streptomuan	5 ml
Amphotericin B	5 ml

Warming of all ingredients to 37 °C, and mixing under sterile conditions.

A.2 Growth medium - CHO-K1 hamster ovary cell line

F-12 Nutrient Mixture	500 ml
L-glutamin	1.7 ml
Tefal Bovine Serum	50 ml
Peericillin/Streptomuan	5 ml
Amphotericin B	5 ml

Warming of all ingredients to 37 °C, and mixing under sterile conditions.

Appendix **B**

Reagents for Comet assay

B.1 1% normal melting agarose gel

SeaKem LE Agarose	800 mg
50x TAE buffer	1.6 ml
dH ₂ O	78.4 ml

Mixing in 100 ml glass. Heat in microwave for ~ 30 sec until it starts to bubble. Important that it does not start to boil.

B.2 1% low melting agarose gel

Ca ²⁺ - and M ²⁺ -free PBS w/ 10mM EDTA	12 ml
Low Melt Agarose	0.12 mg

Mixing in 15 ml tube. Heat up in microwave until it starts to bubble.

B.3 Lysis buffer with 10% DMSO and 1% Triton-X

Stock lysis buffer (4°C)	89 ml
DMSO	10 ml
Triton-X	1 ml

Mixing in glass jar, seal the lid with parafilm.

B.4 Alkali electrophoresis buffer

10 N NaOH (200 g/500 ml dH ₂ O)	30 ml
200 nM EDTA (14.89 g/200 ml dH ₂ O, pH 10)	5.0 ml
dH ₂ O	1000 ml

Per liter: Add 30 ml NaOH and 5.0 ml EDTA to dH₂O, quantity sufficient to 1000 ml, store at RT.

B.5 Neutralizing buffer

Tris base	48.5 g
dH ₂ O	1000 ml
HCl (> 10 M)	

0.4 M Tris: Add 48.5 g Tris base to ~800 ml dH₂O, adjust pH to 7.5 with concentrated (> 10 M) HCl. Add dH₂O to a final volume of 1000 ml, store at RT.

Colocalization images

All images were originally obtained using confocal microscope (Zeiss LSM 5 DUO, Zeiss 510 META, Zeiss LSM 5 Live, Germany). Colocalization was calculated using MATLAB (MathWorks, USA), and based on figures in Sections 4.4 and 4.5. Threshold values were chosen individually for each image by studying its grayscale image in MATLAB.

The staining markers were DRAQ5 (1 μ M, 2 ml, 30 min, 37°C, 5% CO₂) and LysoTracker Red (50 nM, 1 ml, 1 h, 37°C, 5% CO₂).

C.1 F98 rat glioma cells

Chromophores investigated: Ant-OAc ($5\ \mu\text{M}$, 3 ml, 24 h, 37°C , 5% CO_2), Ant-PHEA ($5\ \mu\text{M}$, 3 ml, 24 h, 37°C , 5% CO_2), and $\text{DBB}_2\text{-OAc}$ ($10\ \mu\text{M}$, 3 ml, 24 h, 37°C , 5% CO_2).

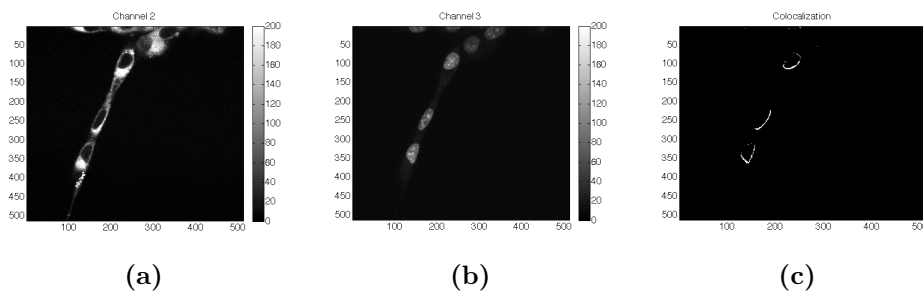


Figure C.1: Colocalization of Ant-OAc with DRAQ5 in F98 cells based on confocal images in Fig. 4.12a. The gray-scale version of the channel 2 image with Ant-OAc in (a), the gray-scale version of the channel 3 image with DRAQ5 in (b), and the binary map of (a) multiplied with (b) (threshold value of > 60 for both) in (c).

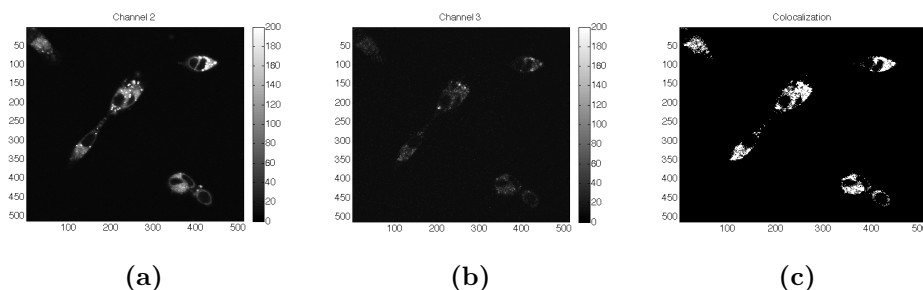


Figure C.2: Colocalization of Ant-OAc with Lysotracker Red in F98 cells based on confocal images in Fig. 4.12b. The gray-scale version of the channel 2 image with Ant-OAc in (a), the gray-scale version of the channel 3 image with Lysotracker Red in (b), and the binary map of (a) multiplied with (b) (threshold value of > 25 for both) in (c).

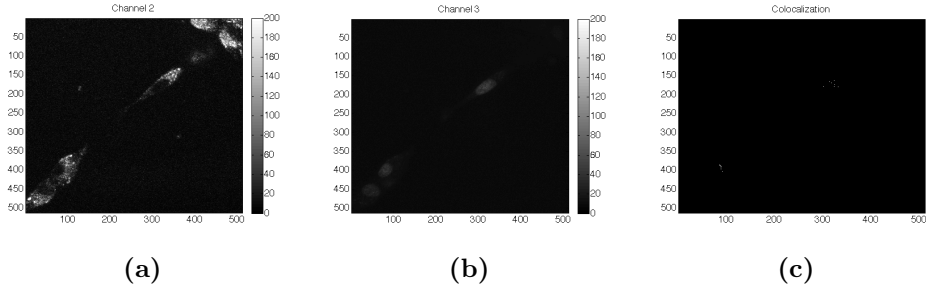


Figure C.3: Colocalization of Ant-PHEA with DRAQ5 in F98 cells based on confocal images in Fig. 4.13a. The gray-scale version of the channel 2 image with Ant-PHEA in (a), the gray-scale version of the channel 3 image with DRAQ5 in (b), and the binary map of (a) multiplied with (b) (threshold value of > 35 for both) in (c).

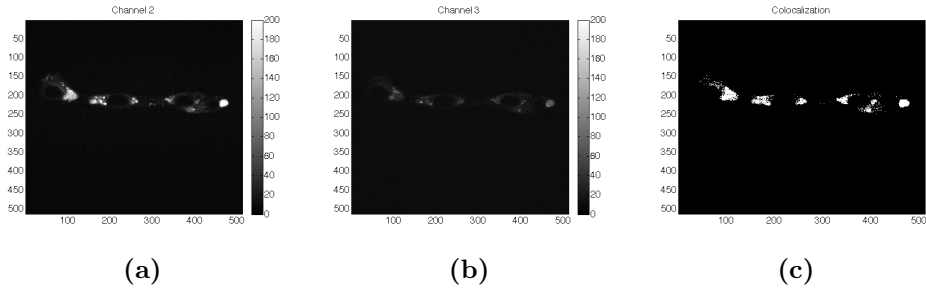


Figure C.4: Colocalization of Ant-PHEA with Lysotracker Red in F98 cells based on confocal images in Fig. 4.13b. The gray-scale version of the channel 2 image with Ant-PHEA in (a), the gray-scale version of the channel 3 image with Lysotracker Red in (b), and the binary map of (a) multiplied with (b) (threshold value of > 25 for both) in (c).

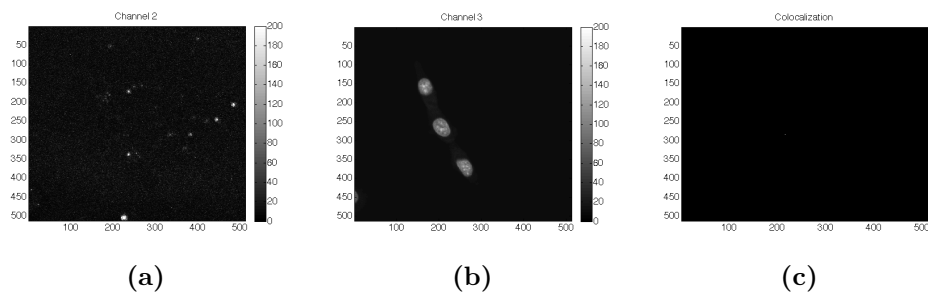


Figure C.5: Colocalization of DBB₂-OAc with DRAQ5 in F98 cells based on confocal images in Fig. 4.14a. The gray-scale version of the channel 2 image with DBB₂-OAc in (a), the gray-scale version of the channel 3 image with Lyso-tracker Red in (b), and the binary map of (a) multiplied with (b) (threshold value of > 60 for (a), and > 40 for (b)) in (c).

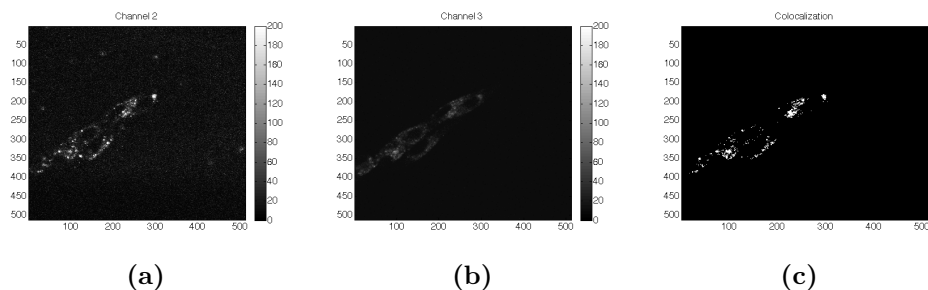


Figure C.6: Colocalization of DBB₂-OAc with DRAQ5 in F98 cells based on confocal images in Fig. 4.14b. The gray-scale version of the channel 2 image with DBB₂-OAc in (a), the gray-scale version of the channel 3 image with Lyso-tracker Red in (b), and the binary map of (a) multiplied with (b) (threshold value of > 50 for (a), and > 30 for (b)) in (c).

C.2 CHO-K1 Chinese hamster ovary cells

Chromophores investigated: Ant-PIm (10 μ M, 2 ml, 24 h, 37°C, 5% CO₂), DBB₂-OAc (10 μ M, 2 ml, 24 h, 37°C, 5% CO₂) and DBB₂-PHEA (50 μ M, 2 ml, 24 h, 37°C, 5% CO₂).

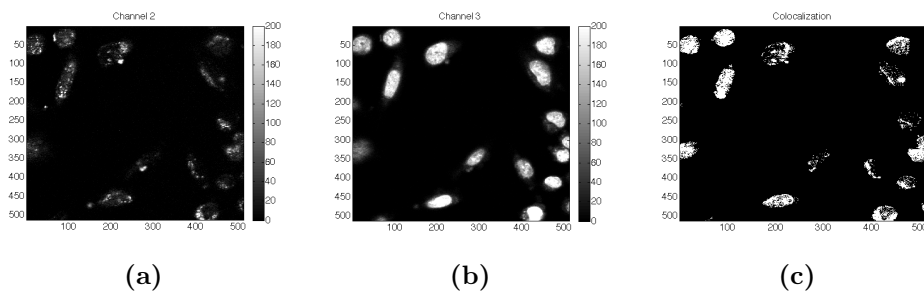


Figure C.7: Colocalization of Ant-PIm with DRAQ5 in CHO-K1 cells based on confocal images in Fig. 4.15a. The gray-scale version of the channel 2 image with Ant-PIm in (a), the gray-scale version of the channel 3 image with DRAQ5 in (b), and the binary map of (a) multiplied with (b) (threshold value of > 20 for (a), and > 50 for (b)) in (c).

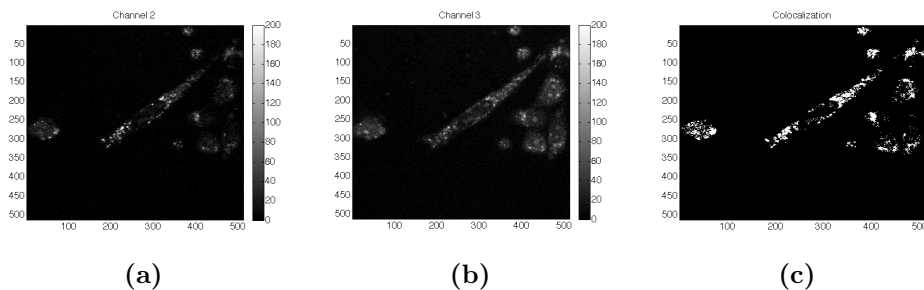


Figure C.8: Colocalization of Ant-PIm with Lysotracker Red in CHO-K1 cells based on confocal images in Fig. 4.15b. The gray-scale version of the channel 2 image with Ant-PIm in (a), the gray-scale version of the channel 3 image with Lysotracker Red in (b), and the binary map of (a) multiplied with (b) (threshold value of > 30 for both) in (c).

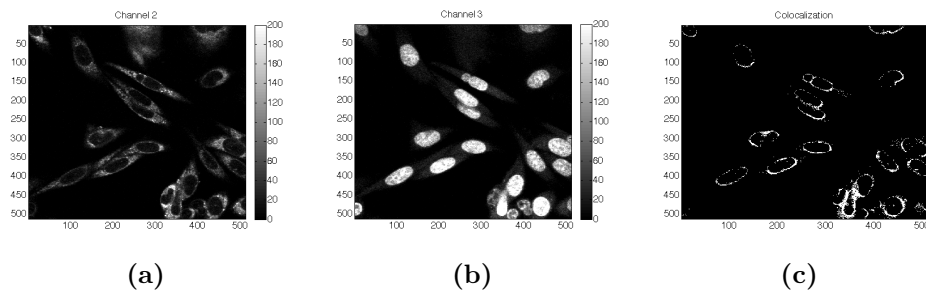


Figure C.9: Colocalization of Ant-PHEA with DRAQ5 in CHO-K1 cells based on confocal images in Fig. 4.17a. The gray-scale version of the channel 2 image with Ant-PHEA in (a), the gray-scale version of the channel 3 image with DRAQ5 in (b), and the binary map of (a) multiplied with (b) (threshold value of > 40 for (a), and > 50 for (b)) in (c).

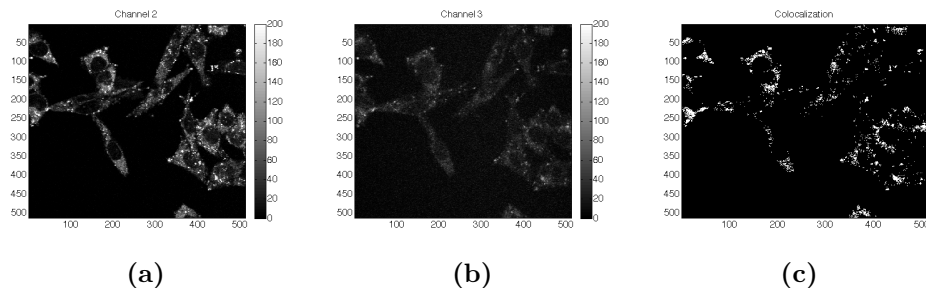


Figure C.10: Colocalization of Ant-PHEA with Lysotracker Red in CHO-K1 cells based on confocal images in Fig. 4.17a. The gray-scale version of the channel 2 image with Ant-PHEA in (a), the gray-scale version of the channel 3 image with Lysotracker Red in (b), and the binary map of (a) multiplied with (b) (threshold value of > 50 for (a), and > 40 for (b)) in (c).

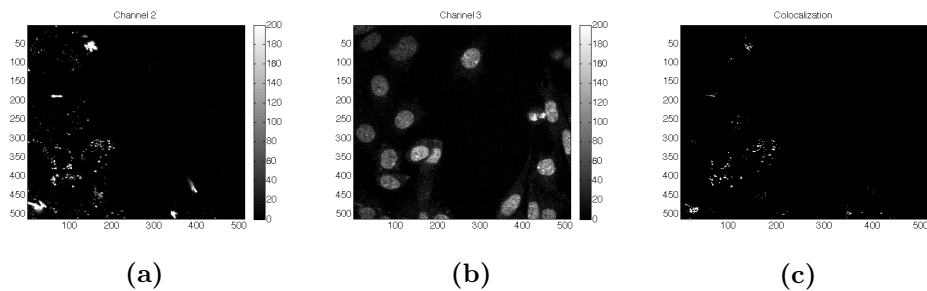


Figure C.11: Colocalization of DBB₂-OAc with DRAQ5 in CHO-K1 cells based on confocal images in Fig. 4.16a. The gray-scale version of the channel 2 image with DBB₂-OAc in (a), the gray-scale version of the channel 3 image with DRAQ5 in (b), and the binary map of (a) multiplied with (b) (threshold value of > 30 for (a), and > 50 for (b)) in (c).

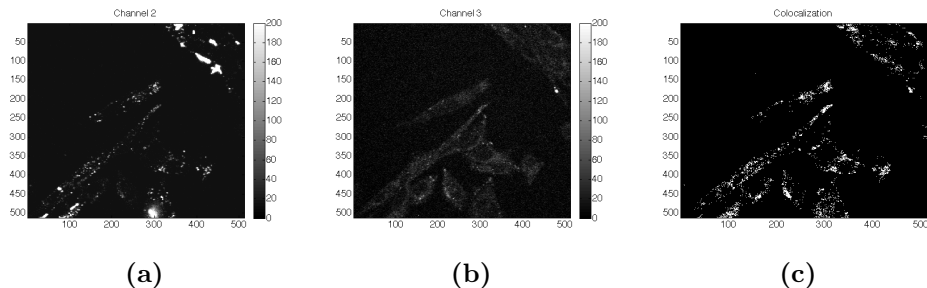


Figure C.12: Colocalization of DBB₂-OAc with Lysotracker Red in CHO-K1 cells based on confocal images in Fig. 4.16b. The gray-scale version of the channel 2 image with DBB₂-OAc in (a), the gray-scale version of the channel 3 image with Lysotracker Red in (b), and the binary map of (a) multiplied with (b) (threshold value of > 30 for both) in (c).

Appendix D

Pilot studies of DBB₂-OAc

Pilot studies of cell survival on rat glioma cancer cells (F98) using MTT assay for varying concentrations of DBB₂-OAc (2.5 μ M, 10 μ M, and 100 μ M; different batches) were conducted by Odrun Gederaas (2013, 2014). Three individually experiments were performed with all samples in duplicates or triplicates. The PCI Biotech LumiSource lamp (Oslo, Norway) with fluence rate of 12.9 mW/cm², and emission at 435 nm was used for all experiments. The results are presented in Fig. D.1.

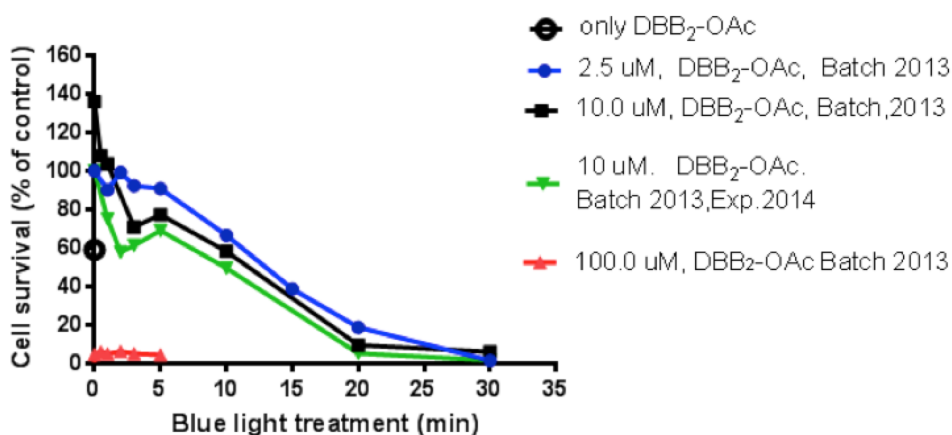


Figure D.1: Cell survival curve for F98 cell line after PDT using DBB₂-OAc (2.5 μ M, 10 μ M, and 100 μ M; different batches). All data points are based on duplicates or triplicates. Dark toxicity (41%) is for 10 μ M DBB₂-OAc.

Appendix **E**

Chromophore synthesis process

Chromophores used in the thesis work were synthesized at ÉNS Lyon by Cyrille Monnereau and his team. The following information describes the synthesis process without detail, and was kindly provided by Bastien Mettra.

The basic steps of synthesis and polymerization are shown in Fig. E.1. The synthesis process of DBB₂-OAc is shown in Fig. E.2, and the synthesis processes from Ant-OAc to Ant-PHEA, and from Ant-PHEA to Ant-PIIm are shown in Fig. E.3.

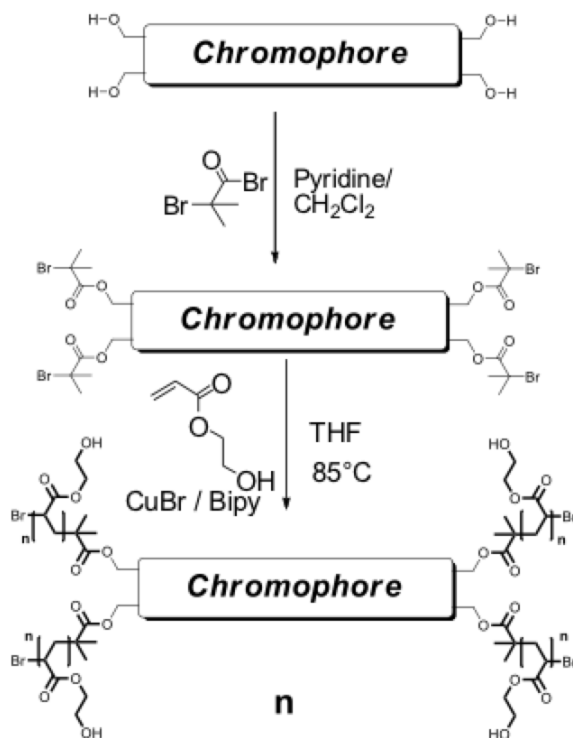


Figure E.1: **First step:** Synthesis of the tetra hydroxy terminated chromophore. **Second step:** Esterification of the chromophore with ATRP initiator. **Third step:** "Oligomerization" with Hydroxyethylacrylate monomer.

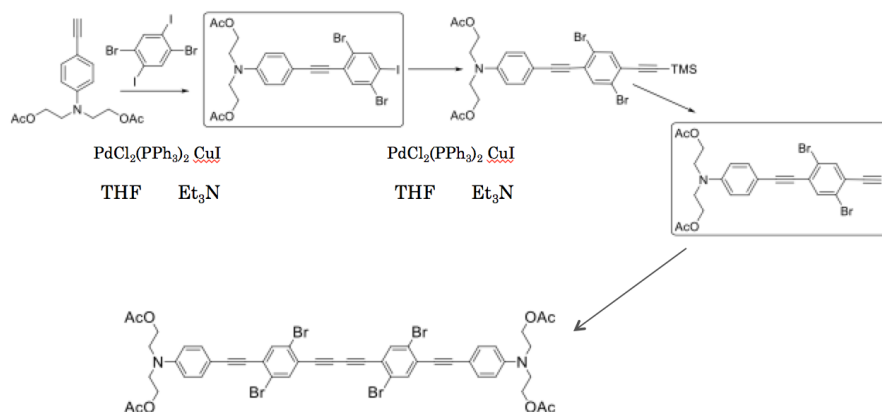


Figure E.2: Synthesis process of DBB₂-OAc.

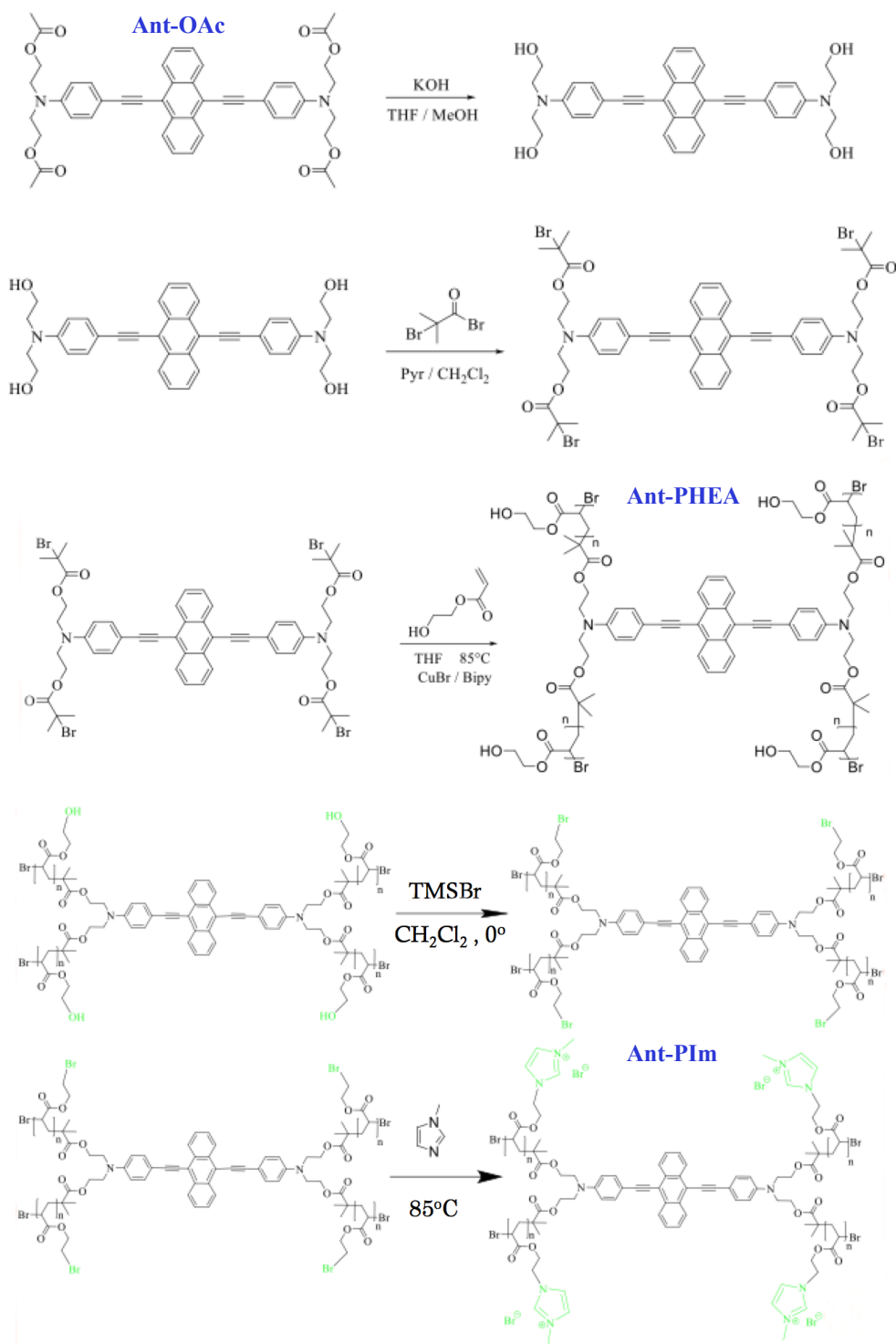


Figure E.3: Synthesis process from Ant-OAc to Ant-PHEA, and from Ant-PHEA to Ant-PIIm.

Appendix F

Bürker chamber

A Bürker chamber was used to count cancer cells before seeding out in dishes or wells (Fig. F.1).

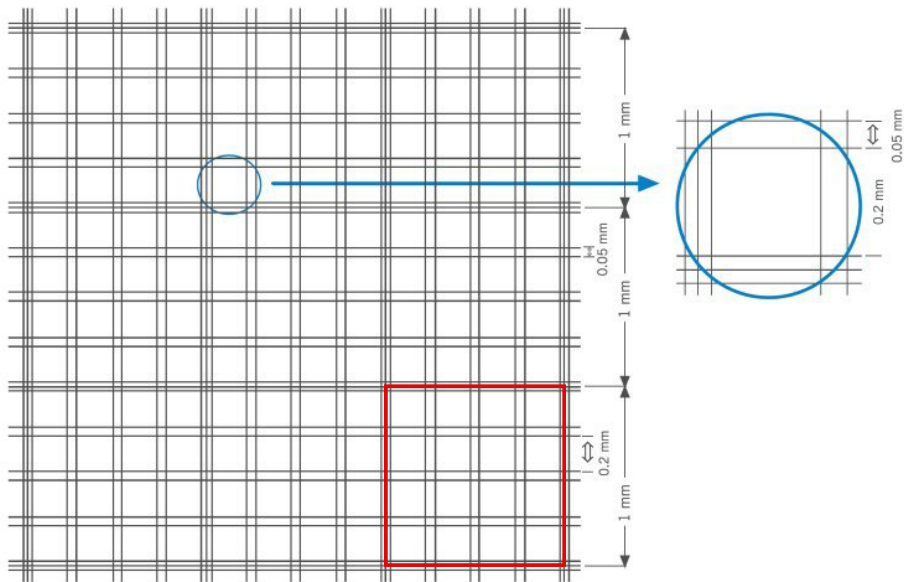


Figure F.1: Sketch of Bürker chamber used for cell counting. The chamber consists of 3x3 A-squares (marked in red), with each A-square being $1 \times 1 \text{ mm}^2$. [64]

Four A-squares (marked as red in Fig. F.1) were counted to find the number of cells per milliliter. The volume is $0.1 \mu\text{l}$ cell suspension per A-square, which

gives the following formula for cell concentration:

$$N_c = \frac{N}{N_A \cdot 0.1 \cdot 10^{-6}} = \frac{N \cdot 10^4}{N_A}, \quad (\text{F.1})$$

where N_c is the cell concentration per ml, N is the number of cells counted, and N_A is the number of counted A-squares. [65]

Appendix **G**

PCI Biotech LumiSource

An excerpt of the PCI Biotech LumiSource manual showing the lamp's emission spectra is attached.

3 Technical information LumiSource®

3.1 Description and components

The LumiSource® is designed specifically to provide homogeneous illumination of living cells in an invitro setting. The lamp consists of light tubes with reflectors designed to provide stable, homogeneous fluency rate over a defined illumination area of 45 x 17 cm. In addition to the tubes, the lamp consists of a removable top plate and a shutter.

The LumiSource® is delivered with a bank of 4 light tubes (4 x 18W Osram L 18/67, Blue) emitting mainly blue light with a peak wavelength of approximately 435 nm.

These light tubes are intended for use in the PCI technology together with the photosensitiser LumiTrans® (supplied by PCI Biotech). The light emission from LumiSource® is selected for optimal excitation of LumiTrans®. (Fig. 1)

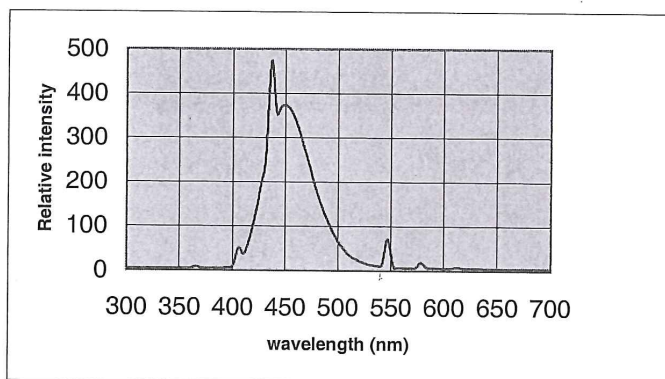


Fig.1 Spectra from standard light tubes (4 x 18W Osram L 18/67, Blue)

3.2 Light emission

It is of great importance that the light emission is stable over the whole illumination area and that the intensity remains stable over time. The variation in light intensity should be minimised in order to get comparable results from experiment to experiment.

The light intensity of LumiSource® varies less than 10% across the illumination area, except for 1 cm from the corners in each direction where the intensity is 15% lower (see Fig. 2-3)

The light emission of the lamp has been measured as indicated in Fig. 2 showing the homogeneity over the light field. The irradiance of the illumination area in the middle of the field is ca. 13.5 mW /cm² (measured by IL 1700 Research Radiometer from International Light).

Note that each lamp will be delivered with information about exact irradiance.

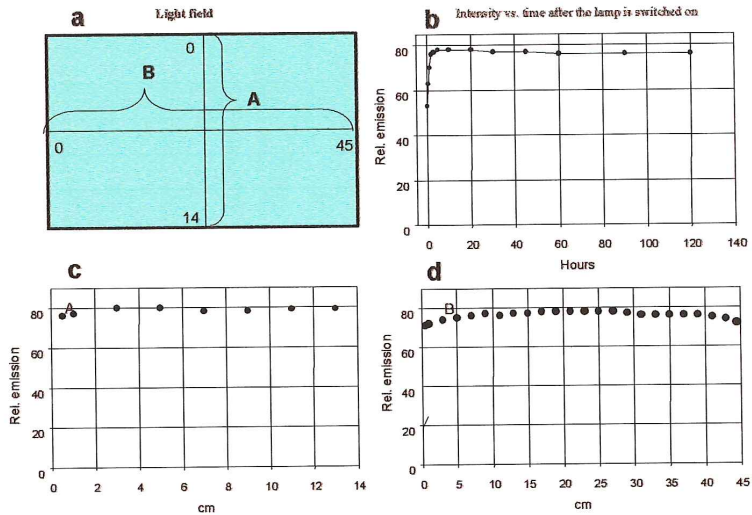


Fig 2. Measurements of relative light emission from the illumination area of LumiSource®. a) shows the illumination area and how light emission has been measured in figure c) and d). The light field in LumiSource® is 14 x 45 cm and the measurements shown in c) and d) were performed as indicated in a). In b) light emission has been measured at different time intervals after the lamp has been switched on. The light emission is stable for at least 24 h after the lamp has been switched on.

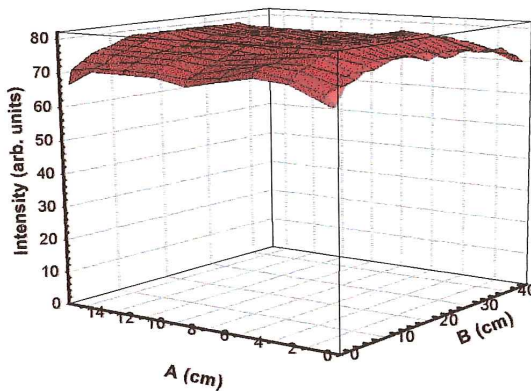


Fig.3. 3D-profile of the light intensity emitted from LumiSource® with A and B as in Fig.2.

3.3 Change of light tubes and filters

If sensitizers that are excited at other wavelengths than around 4-500 nm are used, the standard light tubes can easily be removed and replaced with new tubes.

Removal/change of tubes

Turn off the power and remove the power plug from the socket. Remove the top plate, pull out the shutter, and remove the end reflectors by carefully pulling upwards. Then remove the tubes. Insert new tubes. Place the reflectors and the top plate back and close the shutter. Note that you can only use 18 W light tubes!